

Model-Based Reinforcement Learning for Stochastic Hybrid Systems

Hany Abdulsamad, *Member, IEEE*, and Jan Peters, *Fellow, IEEE*

Abstract—Optimal control of general nonlinear systems is a central challenge in automation. Data-driven approaches to control, enabled by powerful function approximators, have recently had great success in tackling challenging robotic applications. However, such methods often obscure the structure of dynamics and control behind black-box over-parameterized representations, thus limiting our ability to understand the closed-loop behavior. This paper adopts a hybrid-system view of nonlinear modeling and control that lends an explicit hierarchical structure to the problem and breaks down complex dynamics into simpler localized units. Therefore, we consider a sequence modeling paradigm that captures the temporal structure of the data and derive an expectation-maximization (EM) algorithm that automatically decomposes nonlinear dynamics into stochastic piecewise affine dynamical systems with nonlinear boundaries. Furthermore, we show that these time-series models naturally admit a closed-loop extension that we use to extract locally linear or polynomial feedback controllers from nonlinear experts via imitation learning. Finally, we introduce a novel hybrid relative entropy policy search (Hb-REPS) technique that incorporates the hierarchical nature of hybrid systems and optimizes a set of time-invariant local feedback controllers derived from a locally polynomial approximation of a global value function.

Index Terms—Hybrid Systems, State Abstraction, System Identification, Hidden Markov Models, Message Passing, Stochastic Expectation-Maximization, Imitation Learning, Locally Linear Feedback Control, Policy Search.

I. INTRODUCTION

The class of nonlinear dynamical systems governs a vast range of real-world applications and consequently underpins the most challenging problems in classical control, and reinforcement learning (RL) [1], [2]. Recent developments in learning-for-control have pushed towards deploying more complex and highly sophisticated representations, e.g. (deep) neural networks and Gaussian processes, to capture the structure of both dynamics and controllers. This trend led to unprecedented success in the domain of RL [3]. This trend can be observed in both approximate optimal control [4]–[6] and approximate value and policy iteration [7]–[9].

However, before the latest successful revival of neural networks in control and robotics applications, research focused on different paradigms for solving difficult control tasks. One interesting concept relied on decomposing nonlinear structures

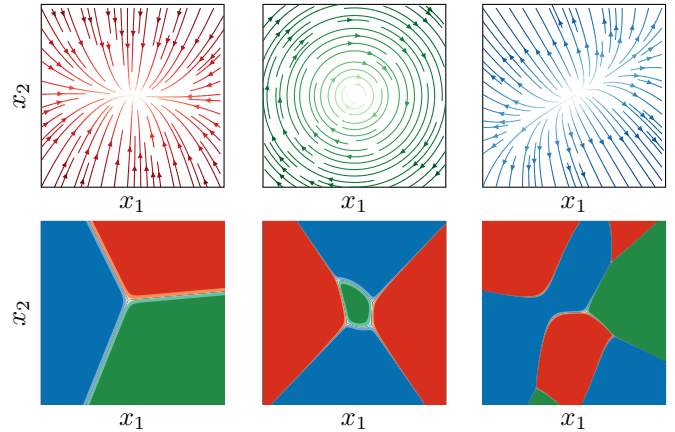


Fig. 1: A hybrid system with $K = 3$ local linear regimes. The top row depicts the mean forced continuous transition dynamics in the phase space. The lower row shows the probability of switching, with corresponding color, as a function of the state. We show different decision boundary models: linear (left), quadratic (middle) and third order polynomial (right).

of dynamics and control into simpler local (linear) components, each responsible for an area of the state-action space. This decomposition is done to preserve interpretability and favorable mathematical properties studied over decades in classical control theory, such as local linear-quadratic assumptions [10]. Instances of this abstraction can be found in the control literature under the labels of hybrid systems or switched models [11]–[14], while in the machine and reinforcement learning communities, the terminology of switching dynamical systems (SDS) and switching state-space models (SSM) is more widely adopted [15]–[18]. Building on this vision, we present in this work a view of data-driven automatic system identification and learning of composite control from the perspective of hybrid systems and switching linear dynamics. We are motivated by recent in-depth analysis of piecewise linear (PWL) activation functions such as rectified linear units (ReLU) [19]–[23], which shows that such representations effectively divide the input space into linear sub-regions. This insight highlights the hierarchical structure hidden between the input and output layers of a neural network and supports viewing them as approximators that rely on local experts. We take this interpretation as an impulse to follow up on ideas from optimal control [24], [25], and reinforcement learning [26], [27], that deviate from fully differentiable paradigms and investigate whether simpler, hybrid discrete-continuous representations may be sufficient for solving certain tasks.

This article was submitted for review on September 1st 2021. This project has received funding from the European Union's Horizon 2020 program under grant agreement No. 640554 (SKILLS4ROBOTS).

H. Abdulsamad and J. Peters are with the Technical University of Darmstadt, Germany (e-mail: hany@robot-learning.de).

Furthermore, the interest in hybrid systems as graphical models is motivated by favorable properties inherent in such representations. On the one hand, hybrid systems allow modeling discrete events, hard nonlinearities, and region-dependent noise. On the other hand, sequence models carry over the advantages of system identification via Bayesian inference and naturally include built-in time recurrency, which captures correlations over extended time horizons.

This paper consolidates prior work on a hierarchical decomposition of nonlinear dynamics [28] and introduces a novel reinforcement learning algorithm for optimizing locally polynomial policies and value functions. In the upcoming sections, we review the literature and highlight the intersection points between prominent paradigms in control and machine learning w.r.t. hybrid systems. Then, we introduce the notation of stochastic switching models and the infinite horizon hybrid control problem. Next, we derive a maximum a posteriori expectation-maximization algorithm for inferring the probabilistic hybrid dynamics. We use this inference procedure in three different scenarios. First, to perform automatic decomposition of nonlinear open-loop dynamics into switching linear regimes with arbitrary boundaries. Second, to deconstruct state-of-the-art nonlinear expert controllers into simpler locally polynomial policies. Finally, We embed the EM procedure into a hybrid policy search algorithm with an explicit discrete-continuous structure. We use this approach to learn hierarchical piecewise polynomial approximations of global value functions and feedback controllers. We empirically evaluate the learned models and policies on a set of numerical examples of stochastic hybrid and nonlinear systems.

II. RELATED WORK

This section reviews work related to modeling and control of hybrid systems and highlights connections and parallels between approaches stemming from the control and machine and reinforcement learning literature.

Hybrid systems have been extensively studied in the control community and are widely used in real-world/real-time applications [29], [30]. However, it is worth noting that most contributions focus on deterministic systems with linear switching boundaries, with the exception of [31], [32], which consider noisy dynamics. For research on the topic of hybrid system identification, we refer to survey work in [33]. The authors introduce a taxonomy of hybrid representations, most importantly piecewise autoregressive exogenous systems (PWARX), and review different procedures commonly used for identifying sub-regimes of dynamics, ranging from mixed-integer optimization [34] to Bayesian methods [35].

Research in the area of optimal control for hybrid systems stretches back to the seminal work of [36], which highlights the possibility of general nonlinear control by considering piecewise linear systems. In [37] an overview of control approaches for piecewise affine switching dynamics is presented. The authors categorize the literature by distinguishing between driven and un-driven systems with externally or internally forced switching mechanisms. Given the global nonlinear behavior of switched systems, the bulk of optimal control

approaches in this area focuses on trajectory optimization methods, which optimize a sequence of actions given a finite horizon objective. Here we highlight the influential work in [38], which formulates the optimal control problem as a mixed-integer quadratic program (MIQP). This approach was later extended in [39] and [40] to solve multi-parametric MIQP and arrive at time-variant locally linear state-feedback controllers and locally quadratic value functions with affine boundaries. Recently, more efficient formulations of finite-horizon hybrid control have been proposed [41]. These algorithms leverage modern techniques from mixed-integer and disjunctive programming and tackle larger-scale problems.

Hybrid representations also play a central role in data-driven, general-purpose process modeling and state estimation [42], [43], where different classes of stochastic hybrid systems serve as powerful generative models for complex dynamical behaviors [44]–[46]. The dominant paradigm in this domain has been that of probabilistic graphical models (PGM), more specifically, hybrid dynamic Bayesian networks (HDBN) for temporal modeling [47], [48]. However, one crucial contribution of recent Bayesian interpretations of switching systems is rooted in the Bayesian nonparametric (BNP) view [49]–[52]. This perspective theoretically allows for an infinite number of components, thus dramatically increasing the expressiveness of such models. Given the limited scope of this review section, we highlight only recent contributions with high impacts, such as [53] and [18], which successfully develop Markov chain Monte Carlo (MCMC) and stochastic variational inference (SVI) techniques for system identification. More recently, the rise of variational auto-encoders [54] has enabled a new and powerful view on inference techniques [55] of hybrid systems. A distinct property of such approaches is their reliance on end-to-end differentiability and the need to relax discrete variables in order to perform inference.

In the domain of learning-for-control, the notion of switching systems is directly related to the paradigm of model-free hierarchical reinforcement learning (HRL) [56], [57], which combines simple representations to build complex policies. Here it is useful to differentiate between two concepts of hierarchical learning, namely *temporal* [58], and *state* abstractions [59]. In their seminal work [60], [61] the authors build on the framework of semi-Markov decision processes (SMDP) [62] to learn activation/termination conditions of temporally extended actions (options) for solving discrete environments. Additionally, pioneering work in optimizing hierarchical control structures with temporally extended actions for robotic applications is developed in [63] specifically, and [64] more broadly. Further recent work has focused on different formulations of the option framework that facilitate simultaneous discovery and learning of options [65]–[69].

However, the concept of state abstraction - the aggregation of state-action spaces into sub-regions, each governed by local dynamics and control - carries the most apparent parallels to the classical view of hybrid systems. In [27], a proof of convergence for RL in tabular environments with state abstraction is presented, while [70] does a comprehensive study of different abstraction schemes and gives a formal definition of the problem. Furthermore, recent work has shown

promising results in solving complex tasks by combining local linear policies, albeit while still leveraging a complex neural network architecture as an upper-level policy [71].

Switching systems also serve as a powerful tool in imitation learning. For example, [72] combines hidden Markov models (HMMs) with Gaussian mixture regression to represent trajectory distributions. In contrast, [67] uses a semi-hidden Markov model (HSMM) to learn hierarchical policies, and [73] introduces switching density networks for system identification and behavioral cloning. Finally, a fully Bayesian framework for hierarchical decomposition of policies is presented in [74], albeit while considering known transition dynamics.

In light of the reviewed literature, we highlight the main differences that distinguish this paper from the approaches mentioned above. First, this work leverages probabilistic hybrid dynamic networks as hierarchical representations of nonlinear open- and closed-loop behaviors. Contrary to standard PWARX, HDBN can easily integrate stochasticity and nonlinear switching boundaries, leading to more refined and less redundant segmentation of the state-action space. Furthermore, by pursuing an abstraction over the states instead of time, we circumvent the need to infer so-called termination policies, a characteristic of the option framework. Finally, the proposed hybrid policy search approach formulates a non-convex infinite horizon objective that optimizes a hierarchical locally polynomial approximation of the value function. This approximation is used to derive stationary switching feedback controllers. In contrast, trajectory optimization and model predictive control techniques are often limited to quadratic programming scenarios and optimize a finite horizon objective that yields time-variant value functions and controllers.

III. PROBLEM STATEMENT

Consider the time-discrete optimal control problem of a stochastic nonlinear dynamical system to be defined as an infinite horizon Markov decision processes (MDP). An MDP is a mathematical abstraction of an environment defined over a state space $\mathcal{X} \subseteq \mathbb{R}^d$ and an action space $\mathcal{U} \subseteq \mathbb{R}^m$. The probability of a state transition from state \mathbf{x} to state \mathbf{x}' by applying action \mathbf{u} is governed by the Markovian time-independent density function $p(\mathbf{x}'|\mathbf{x}, \mathbf{u})$. The reward $r(\mathbf{x}, \mathbf{u})$ is a function of the state \mathbf{x} and action \mathbf{u} and is discounted over time by a factor $\vartheta \in [0, 1)$. The state-dependent policy $\pi(\mathbf{u}|\mathbf{x})$, from which the actions are drawn, is a density determining the probability of an action \mathbf{u} given a state \mathbf{x} . The general objective in an infinite horizon optimal control problem is to maximize the expected cumulative sum of discounted rewards $V^\pi(\mathbf{x}) = \mathbb{E}[\sum_t \vartheta^t r]$, where V^π is denoted as the state-value function under the policy π .

Given the context of this work and our choice to model the system with switching linear models, we introduce to the MDP formulation a new hidden discrete variable \mathbf{z} , an indicator of the currently active linear regime. The resulting transition dynamics can then expressed by a factorized density function $p(\mathbf{x}', \mathbf{z}'|\mathbf{x}, \mathbf{u}, \mathbf{z}) = p(\mathbf{z}'|\mathbf{z}, \mathbf{x}, \mathbf{u})p(\mathbf{x}'|\mathbf{x}, \mathbf{u}, \mathbf{z}')$, which we depict as a graphical model in Figure 2 and discuss in further detail in the upcoming section. In the same spirit of

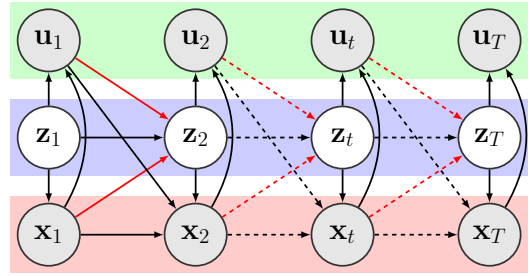


Fig. 2: Graphical model of recurrent autoregressive hidden Markov models (rARHMMs) extended to support hybrid controls. rARHMMs are hybrid dynamic Bayesian networks that explicitly allow the discrete state \mathbf{z} to depend on the continuous variables \mathbf{x} and \mathbf{u} , as highlighted in red.

simplification through hierarchical modeling, we employ a mixture of switching linear controllers $\pi(\mathbf{u}|\mathbf{x}, \mathbf{z})$. The resulting framework becomes a combination of filtering to infer the active local dynamics denoted by \mathbf{z} , and optimal control to apply appropriate actions \mathbf{u} given \mathbf{x} and \mathbf{z} .

IV. HYBRID DYNAMIC BAYESIAN NETWORKS

We focus on recurrent autoregressive hidden Markov models (rARHMMs) as a representation of closed-loop stochastic hybrid systems. The rARHMM is a special case of recurrent switching linear dynamical systems (rSLDS) [18], also known as augmented SLDS [75]. In contrast to rSLDS, an rARHMM lacks an observation model and directly describes the internal state with an additive noise process. We extend rARHMMs to support exogenous and endogenous inputs in order to simulate the open- and closed-loop behaviors of driven dynamics. Figure 2 depicts the corresponding graphical model, which closely resembles the linear-boundary PWARX.

An rARHMM with K regions models the trajectory of a hybrid system as follows. The initial continuous state $\mathbf{x}_1 \in \mathbb{R}^d$ and continuous action $\mathbf{u}_1 \in \mathbb{R}^m$ are drawn from a pair of Gaussian and conditional Gaussian distributions¹, respectively. The initial discrete indicator \mathbf{z}_1 is a one-hot random vector modeled by a categorical density parameterized by $\boldsymbol{\pi}$

$$\mathbf{z}_1 \sim \text{Cat}(\boldsymbol{\pi}), \quad \mathbf{x}_1 \sim \mathcal{N}(\boldsymbol{\mu}_{z_1}, \boldsymbol{\Lambda}_{z_1}), \quad \mathbf{u}_1 \sim \mathcal{N}(\mathbf{K}_{z_1}\phi(\mathbf{x}_1), \boldsymbol{\Delta}_{z_1}).$$

The transition of the continuous state \mathbf{x}_{t+1} and actions \mathbf{u}_t are modeled by linear-Gaussian dynamics

$$\begin{aligned} \mathbf{x}_{t+1} &= \mathbf{A}_{z_{t+1}}\mathbf{x}_t + \mathbf{B}_{z_{t+1}}\mathbf{u}_t + \mathbf{c}_{z_{t+1}} + \boldsymbol{\lambda}_t, & \boldsymbol{\lambda}_t &\sim \mathcal{N}(\mathbf{0}, \boldsymbol{\Lambda}_{z_{t+1}}), \\ \mathbf{u}_t &= \mathbf{K}_{z_t}\phi(\mathbf{x}_t) + \boldsymbol{\delta}_t, & \boldsymbol{\delta}_t &\sim \mathcal{N}(\mathbf{0}, \boldsymbol{\Delta}_{z_t}), \end{aligned}$$

where $(\mathbf{A}, \mathbf{B}, \mathbf{c}, \mathbf{K}, \boldsymbol{\Lambda}, \boldsymbol{\Delta})$ are matrices and vectors of appropriate dimensions w.r.t. \mathbf{x} and \mathbf{u} , $\forall k \in [1, K]$. $\phi(\mathbf{x})$ are affine polynomial state features of arbitrary order. The discrete transition probability $p(\mathbf{z}_{t+1}|\mathbf{z}_t, \mathbf{x}_t, \mathbf{u}_t)$ is governed by K categorical distributions parameterized by state-action dependent multi-class logistic functions

$$\chi_{ij} = p(\mathbf{z}_{t+1} = j|\mathbf{z}_t = i, \mathbf{x}_t, \mathbf{u}_t)^2 \propto \exp(f(\mathbf{x}_t, \mathbf{u}_t; \boldsymbol{\omega}_{ij})),$$

where f may have any type of \mathbf{x} and \mathbf{u} features, e.g.

¹We parameterize all Gaussian distribution by their precision matrices instead of the more common definition with covariances.

²We abuse notation slightly by sometimes using \mathbf{z} to refer to the discrete state index, instead of treating it as a one-hot vector.

polynomial or neural. A set of vectors ω_{ij} parameterize all transition combinations $i \rightarrow j \forall i, j \in [1, K]$. Figure 1 depicts realizations of different transition functions that lead to a variety of state space decompositions.

This representation of switching dynamics has a significant advantage over other non-recurrent hybrid models [53], [76], since it couples discrete and continuous dynamics of an HMM in both directions. This aspect has significant implications on the model’s expressiveness and ability to capture the underlying dynamics of interesting physical applications, as it limits redundancies in the hierarchical decomposition of the state-action space. For example, one may consider a case in which one component can explain the local dynamics in the neighborhood of multiple non-connected discrete states. However, to achieve a sharp decision boundary in such scenarios, a non-recurrent model has to duplicate the continuous dynamics with a different transition probability for each set of neighboring regions. This duplication leads to redundant discrete states with the same continuous dynamics while differing in their switching behavior. One approach to circumvent this explosion is to consider a hierarchical abstraction over meta regions similar to factorial hidden Markov model (FHMM) [77]. Nonetheless, such representations may still require multiple hierarchy levels to match the expensiveness of a recurrent transition, which compactly parameterizes a continuum of probabilities.

However, at the same time, the discrete-continuous coupling introduces inter-dependencies between \mathbf{z} , \mathbf{x} and \mathbf{u} , which in the case of rSLDS, make exact filtered and smoothed inference intractable [47], [48]. This issue arises because the hidden state of an rSLDS becomes a mixture over \mathbf{x} and \mathbf{z} , whose number of components explodes exponentially when propagated in time [75]. Moreover, (r)SLDS are not uniquely identifiable due to rotational invariance [78]. These two limitations have informed our decision to focus on rARHMM as a first step since they admit tractable filtering and smoothing over the hidden state \mathbf{z} , as the upcoming section will reveal.

The remainder of this paper focuses on using these hybrid models in two ways. First, an open-loop setting that treats the control \mathbf{u} as an exogenous input and is used for automatic identification of nonlinear systems via decomposition into continuous and discrete switching dynamics. Here we assume all regions to be first-order Markovian linear systems. Second, a closed-loop setting that assumes the control \mathbf{u} to originate from a nonlinear controller. We show that this setting can decompose both dynamics and control simultaneously in an imitation learning scenario. Additionally, we leverage the same framework in a hybrid reinforcement learning algorithm to learn switching controllers of general nonlinear systems.

V. HIERARCHICAL REINFORCEMENT LEARNING FOR HYBRID DYNAMICAL SYSTEMS

In our review of related work in Section II, we highlight that many successful classical hybrid control algorithms are limited to the finite-horizon setting and rely on trajectory-based time-variant policies. This type of controllers is disadvantageous in applications that require a reactive stationary feedback

controller with broad coverage over the state-action space. These formulations’ main drawback is their reliance on linear separation boundaries of the hybrid dynamics. On the other hand, we mention several RL-based approaches that learn global time-invariant policies. However, these algorithms are exclusively model-free and mostly rely on time-abstraction paradigms, which require learning task-specific termination policies, in addition to the local controllers.

In this section, we present a stochastic infinite horizon sample-based optimization technique that leverages the structure and properties of hybrid systems under the paradigm of state abstraction. Our algorithm extends the step-based formulation of relative entropy policy search (REPS) [79]–[81] by introducing a discrete state variable \mathbf{z} and taking into account the structure of hybrid dynamics. Our approach, hybrid REPS (Hb-REPS), leverages the state-action-dependent nonlinear switches $p(\mathbf{z}'|\mathbf{z}, \mathbf{x}, \mathbf{u})$ as a task-independent upper-level coordinator to a mixture of K lower-level stationary linear (polynomial) policies $\pi(\mathbf{u}|\mathbf{x}, \mathbf{z})$. While the proposed approach shares many features with [67], our formulation relies on a state-abstraction representation of hybrid systems and embeds the hierarchical model structure into the optimization problem in order to learn a hierarchy over the global value function. In contrast, [67] operates in the framework of semi-Markov decision processes and optimizes a mixture over termination and feedback policies without considering the existence of a hierarchy over the dynamics and value function.

A. Infinite-Horizon Stochastic Hybrid Control

In the REPS framework an optimal control problem is presented as an iterative trust-region optimization for a discounted average-reward objective under a stationary state-action distribution $\pi(\mathbf{u}|\mathbf{x}, \mathbf{z})\mu(\mathbf{x}, \mathbf{z})$, Equation (1a). The trust-region is formulated as a Kullback-Leibler divergence (KL) [82], Equation (1c). The purpose of the KL-constraint is to bound the information loss between iterations, given the data-driven and statistical nature of the approach. The REPS formulation explicitly incorporates a dynamics consistency constraint, Equation (1b), that describes how the stochastic state of the system evolves. This property motivated our algorithmic choice when integrating the hybrid dynamics. The following describes the optimization solved during a single iteration of what we refer to as hybrid REPS

$$\max_{\pi, \mu} J = \sum_{\mathbf{z}} \iint r(\mathbf{x}, \mathbf{u}, \mathbf{z}) \pi(\mathbf{u}|\mathbf{x}, \mathbf{z}) \mu(\mathbf{x}, \mathbf{z}) \, \mathrm{d}\mathbf{u} \, \mathrm{d}\mathbf{x}, \quad (1a)$$

$$\text{s. t.} \quad \mu(\mathbf{x}', \mathbf{z}') = (1 - \vartheta) \mu_1(\mathbf{x}', \mathbf{z}') + \vartheta \sum_{\mathbf{z}} \iint \pi(\mathbf{u}|\mathbf{x}, \mathbf{z}) \mu(\mathbf{x}, \mathbf{z}) p(\mathbf{x}', \mathbf{z}'|\mathbf{x}, \mathbf{u}, \mathbf{z}) \, \mathrm{d}\mathbf{u} \, \mathrm{d}\mathbf{x}, \quad (1b)$$

$$\text{KL}(\pi(\mathbf{u}|\mathbf{x}, \mathbf{z}) \mu(\mathbf{x}, \mathbf{z}) \parallel q(\mathbf{x}, \mathbf{u}, \mathbf{z})) \leq \epsilon, \quad (1c)$$

$$\sum_{\mathbf{z}} \iint \pi(\mathbf{u}|\mathbf{x}, \mathbf{z}) \mu(\mathbf{x}, \mathbf{z}) \, \mathrm{d}\mathbf{u} \, \mathrm{d}\mathbf{x} = 1, \quad (1d)$$

where $\mu(\mathbf{x}, \mathbf{z})$ is the optimal stationary mixture distribution, $q(\mathbf{x}, \mathbf{u}, \mathbf{z})$ is the trust-region reference distribution, and the constraint in Equation (1d) guarantees the normalization of

the state-action distribution. The factor $1 - \vartheta$ represents the probability of an infinite process to reset back to an initial distribution $\mu_1(\mathbf{x}, \mathbf{z})$. The notion of resetting is necessary to ensure ergodicity and allows the interpretation of ϑ as a discount factor and regularization of the MDP [81], [83].

B. Optimality Conditions and Dual Optimization

For convenience, let $p(\mathbf{x}, \mathbf{u}, \mathbf{z}) = \pi(\mathbf{u}|\mathbf{x}, \mathbf{z})\mu(\mathbf{x}, \mathbf{z})$ for which the marginalization identity $\int p(\mathbf{x}, \mathbf{u}, \mathbf{z}) d\mathbf{u} = \mu(\mathbf{x}, \mathbf{z})$ holds. Using the method of Lagrangian multipliers [84], we can solve the constrained primal problem w.r.t. state-action distribution $p(\mathbf{x}, \mathbf{u}, \mathbf{z})$

$$p^*(\mathbf{x}, \mathbf{u}, \mathbf{z}) \propto q(\mathbf{x}, \mathbf{u}, \mathbf{z}) \exp \left[\frac{A(\mathbf{x}, \mathbf{u}, \mathbf{z}, V)}{\eta} \right], \quad (2)$$

where η is the Lagrangian variable associated with Equation (1c) and $A(\mathbf{x}, \mathbf{u}, \mathbf{z}, V)$ the advantage function given as

$$\begin{aligned} A &= r(\mathbf{x}, \mathbf{u}, \mathbf{z}) + (1 - \vartheta) \sum_{\mathbf{z}'} \int V(\mathbf{x}', \mathbf{z}') \mu_1(\mathbf{x}', \mathbf{z}') d\mathbf{x}' \quad (3) \\ &+ \vartheta \sum_{\mathbf{z}'} \int V(\mathbf{x}', \mathbf{z}') p(\mathbf{x}', \mathbf{z}'|\mathbf{x}, \mathbf{u}, \mathbf{z}) d\mathbf{x}' - V(\mathbf{x}, \mathbf{z}) \\ &= Q(\mathbf{x}, \mathbf{u}, \mathbf{z}) - V(\mathbf{x}, \mathbf{z}). \end{aligned}$$

The functions $V(\mathbf{x}, \mathbf{z})$ and $Q(\mathbf{x}, \mathbf{u}, \mathbf{z})$ are the state- and state-action value functions, respectively. The function $V(\mathbf{x}, \mathbf{z})$ appears naturally in REPS as the Lagrangian function associated with Equation (1b). The full Lagrangian of the primal can be found in Appendix III. By substituting the optimal parameter p^* back into the Lagrangian and factorizing $q(\mathbf{x}, \mathbf{u}, \mathbf{z})$, we arrive at the dual function G as a function of the remaining Lagrangian variables η and V

$$G = \eta\epsilon + \eta \log \iint q(\mathbf{x}, \mathbf{u}) \sum_{\mathbf{z}} q(\mathbf{z}|\mathbf{x}, \mathbf{u}) \exp \left[\frac{A(V|\cdot)}{\eta} \right] d\mathbf{u} d\mathbf{x},$$

where $q(\mathbf{z}|\mathbf{x}, \mathbf{u})$ is the posterior over \mathbf{z} given the observations \mathbf{x} and \mathbf{u} . In Section VI, we derive a forward-backward algorithm for inferring these probabilities, allowing us to compute the expectation over \mathbf{z} . The expectations over \mathcal{X} and \mathcal{U} are usually analytically intractable, therefore, we approximate them given samples from the reference distribution $q(\mathbf{x}, \mathbf{u})$. The multipliers η and V are then obtained by numerically minimizing the dual $G(\eta, V)$

$$\arg \min_{\eta, V} G(\eta, V), \quad \text{s. t.} \quad \eta \geq 0,$$

which acts as the upper bound on the primal objective.

C. Modeling Local Dynamics and State-Value Function

Up to this point the derivation has been generic. We have made no assumptions on the dynamics $p(\mathbf{x}', \mathbf{z}'|\mathbf{x}, \mathbf{u}, \mathbf{z})$ or value function $V(\mathbf{x}, \mathbf{z})$. Now we introduce the local Gaussian linear dynamics and logistic switching described in Section IV and assume these representations to be available in parametric form at this point³. Furthermore, we model the state-value function with local n -th degree polynomial functions $V(\mathbf{x}, \mathbf{z}) =$

$\omega_{\mathbf{z}}^{\top} \phi_{\mathbf{z}}(\mathbf{x})$, where $\phi(\mathbf{x})$ is the state-feature vector and which contain all possible polynomial features of the state \mathbf{x} and $\omega_{\mathbf{z}}$ is the parameter vector assigned to the different linear regions.

Given the stochastic model of local dynamics $p(\mathbf{x}'|\mathbf{x}, \mathbf{u}, \mathbf{z})$ and locally polynomial value function $V(\mathbf{x}', \mathbf{z}')$, we can analytically determine the necessary expectations over the future state \mathbf{x}' and initial state \mathbf{x}_1 in Equation (3)

$$\begin{aligned} \mathbb{E}_{\mathbf{x}', \mathbf{z}'} [V(\mathbf{x}', \mathbf{z}')] &= \sum_{\mathbf{z}'} \int V(\mathbf{x}', \mathbf{z}') p(\mathbf{x}', \mathbf{z}'|\mathbf{x}, \mathbf{u}, \mathbf{z}) d\mathbf{x}', \\ \mathbb{E}_{\mathbf{x}_1, \mathbf{z}_1} [V(\mathbf{x}', \mathbf{z}')] &= \sum_{\mathbf{z}'} p(\mathbf{z}'|\mathbf{x}') \int V(\mathbf{x}', \mathbf{z}') \mu_1(\mathbf{x}') d\mathbf{x}', \end{aligned}$$

where $p(\mathbf{z}'|\mathbf{x}, \mathbf{u}, \mathbf{z})$ and $p(\mathbf{z}'|\mathbf{x}')$ again correspond to the posterior probabilities of \mathbf{z} .

These models enable our approach to capture the stochasticity of the system when approximating the discounted future returns and to deliver an estimation of the advantage function $A(\mathbf{x}, \mathbf{u})$ in contrast to the TD-error $\delta(\mathbf{x}, \mathbf{u})$ in the general REPS framework. Here we consider that the integral over the polynomial terms of $V(\mathbf{x}', \mathbf{z}')$ can be interpreted as the linear combination of the 0-th to n -th order (non-central) moments of a Gaussian-distributed random variable \mathbf{x}' .

For a unifying derivation of the analytical form of those expectations for any n -th order polynomial, we apply the method of moment-generating functions [85]. The moment-generating function of a multivariate-Gaussian with mean $\boldsymbol{\mu}$ and covariance matrix $\boldsymbol{\Sigma}$ is given by

$$M_{\mathbf{x}'}(\mathbf{t}) = \exp \left[\mathbf{t}^{\top} (\boldsymbol{\mu} + \frac{1}{2} \boldsymbol{\Sigma} \mathbf{t}) \right],$$

which renders possible to calculate arbitrary n -th non-central moments m_n by evaluating the n -th partial derivative of $M_{\mathbf{x}'}(\mathbf{t})$ evaluated at $\mathbf{t} = 0$

$$m_n = \mathbb{E}[(\mathbf{x}')^n] = \left. \frac{\partial^n M_{\mathbf{x}'}}{\partial \mathbf{t}^n} \right|_{\mathbf{t}=0}.$$

Finally, it is worth mentioning that the previous expectation may also be approximated numerically by generating and averaging over samples from the modeled joint densities $p(\mathbf{x}', \mathbf{z}'|\mathbf{x}, \mathbf{u}, \mathbf{z})$ and $p(\mathbf{z}_1, \mathbf{x}_1)$.

D. Stationarity of Distribution Mixtures

The dynamics Equation (1b), which ensures the stationarity of $\mu(\mathbf{x}, \mathbf{z})$, uncovers an interesting aspect of our optimization problem. A careful inspection of that integral equation reveals that a mixture distribution $\mu(\mathbf{x}, \mathbf{z})$ propagated through the mixture dynamics $p(\mathbf{x}', \mathbf{z}'|\mathbf{x}, \mathbf{u}, \mathbf{z})$ results in a mixture $\mu(\mathbf{x}', \mathbf{z}')$ that keeps growing with every pass, leading to an explosion in the number of components of the joint state distribution. This problem highlights a crucial computational issue of trajectory-based optimal control approaches of stochastic hybrid systems, as it becomes expensive to maintain the full mixture state distribution $\mu(\mathbf{x}, \mathbf{z})$ after several time steps. Common solutions to this issue usually involve falling back to crude Gaussian mixture reduction techniques [86] that inadvertently sacrifice information and blur the distribution.

³In Section VI, we present a maximum a posteriori expectation-maximization procedure that infers the model parameters from data.

This consideration has motivated us to formulate the optimal control problem as one that focuses on finding a stationary solution for $\mu(\mathbf{x}, \mathbf{z})$. We hypothesize, that including Equation (1b) as a constraint leads to an optimal mixture policy $\pi(\mathbf{u}|\mathbf{x}, \mathbf{z})$ that acts as a *filter* and *dampens* certain modes of $\mu(\mathbf{x}', \mathbf{z}')$ with little contribution to the average-reward objective. However, we recognize that a more in-depth analysis of the nature of this integral equation is necessary.

E. Maximum-A-Posteriori Policy Improvement

Another important advantage of this model-based approach becomes evident when considering the policy improvement step in the REPS framework. The policy update is incorporated into the optimality condition of the stationary state-action distribution $p(\mathbf{x}, \mathbf{u}, \mathbf{z}) = \pi(\mathbf{u}|\mathbf{x}, \mathbf{z})\mu(\mathbf{x}, \mathbf{z})$ in Equation (2). As a consequence, updating the mixture policies $\pi(\mathbf{u}|\mathbf{x}, \mathbf{z})$ requires the computation of state probabilities $\mu(\mathbf{x}, \mathbf{z})$, which in turn require knowledge of the dynamics model. This issue is circumvented in other model-free realizations of REPS by introducing a crude approximation to enable a model-free policy update nonetheless. In [87], the authors postulate that the new state distribution $\mu(\mathbf{x}, \mathbf{z})$ is usually “close enough” to the old distribution $q(\mathbf{x}, \mathbf{z})$, thus allowing the ratio $q(\mathbf{x}, \mathbf{z})/\mu(\mathbf{x}, \mathbf{z})$ to be ignored when a weighted maximum-likelihood fit of the actions \mathbf{u} is performed to update π .

While the assumption of “closeness” may be practical and empowers many successful flavors of REPS, it is crucial to be aware of its technical ramifications, as it undermines the primary motivation of a relative entropy bound on the state-action distribution in Equation (1c). This aspect is unique in the REPS framework when compared to other state-of-the-art approximate policy iteration algorithms [7], [9], [88], that optimize a similar objective, albeit with a relaxed bound that only limits the change of the action distribution π .

In contrast, our proposed algorithm leverages the modeled continuous-discrete dynamics and updates the controllers $\pi(\mathbf{u}|\mathbf{x}, \mathbf{z})$ via an importance-weighted maximum a posteriori optimization. Consequently, the optimality condition in Equation (2) is satisfied by deriving a Baum-Welch expectation-maximization procedure, Section VI, to fit a closed-loop rARHMM to the joint state-action distribution $q(\mathbf{x}, \mathbf{u}, \mathbf{z})$, weighted by the exponentiated advantage function $A(\mathbf{x}, \mathbf{u}, \mathbf{z})$. An analogous approach based on time-abstracted semi-Markov processes and lacking prior regularization is used in [67].

VI. BAYESIAN INFERENCE OF SWITCHING DYNAMICS AND CONTROL

In this section, we sketch the outline of an expectation-maximization/Baum-Welch algorithm [89]–[91] for inferring the parameters θ of an rARHMM given time-series observations \mathbf{X}, \mathbf{U} . Our approach is related in some aspects to the Baum-Welch algorithms proposed in [92] and [67]. However, we introduce suitable priors over all parameters and derive a maximum a posteriori (MAP) technique with a stochastic maximization step and hyperparameter optimization. In our experience, the priors and noisy gradient estimate significantly reduce the sensitivity of EM w.r.t. initialization and appear to

be less prone to get stuck in bad local minima - an effect well-studied in neural networks [93].

Note that, although our procedure is not fully Bayesian like methods that rely on Gibbs sampling [18], [53], it does have computational and predictive advantages. On the one hand, Gibbs sampling can suffer from slow convergence in high dimensional spaces leading to an overall high computational cost [94]. On the other hand, a good prior specification is crucial in small data regimes, where a vague prior may dominate the predictive posterior and effectively cause underfitting. Our proposed hyperparameter optimization elevates this concern by optimizing the prior parameters via empirical Bayes [95], thus attenuating the prior influence and improving the predictive performance significantly. Another drawback of Gibbs sampling-based approaches is their inflexibility in incorporating powerful neural transition predictor functions due to their reliance on conditionally conjugate computation.

A. Maximum A Posteriori Optimization

Consider again the rARHMM in Figure 2 where the continuous state \mathbf{x} and action \mathbf{u} are observed variables, while the K -region indicators \mathbf{z} are hidden. To infer the model parameters, we consider a dataset consisting of N state-action trajectories $\mathcal{D} = \{(\mathbf{X}^n, \mathbf{U}^n)\}_{n=1}^N$, each of length T , where \mathbf{X}^n , \mathbf{U}^n and \mathbf{Z}^n represent an entire trajectory. The inference objective for system identification is to maximize the log-posterior probability of the observed trajectories $\mathbf{X}^n, \mathbf{U}^n$ conditioned on the free parameters $\theta = \{\pi, \mu_{1,k}, \Lambda_{1,k}, \mathbf{A}_k, \mathbf{B}_k, \mathbf{c}_k, \Lambda_k, \mathbf{K}_k, \Delta_k, \omega_{ik}\} \forall i, k \in [1, K]$

$$\theta_{\text{MAP}} := \arg \max_{\theta} \log \prod_{n=1}^N \sum_{\mathbf{z}^n} p(\mathbf{X}^n, \mathbf{U}^n, \mathbf{Z}^n | \theta) p(\theta), \quad (4)$$

where $p(\mathbf{X}^n, \mathbf{U}^n, \mathbf{Z}^n | \theta)$ is the complete-data likelihood of a single trajectory and factorizes according to

$$\begin{aligned} p(\cdot | \theta) &= p(\mathbf{z}_1^n) p(\mathbf{x}_1^n | \mathbf{z}_1^n) p(\mathbf{u}_1^n | \mathbf{z}_1^n) \\ &\times \prod_{t=2}^T p(\mathbf{x}_t^n | \mathbf{x}_{t-1}^n, \mathbf{u}_{t-1}^n, \mathbf{z}_t^n) p(\mathbf{u}_t^n | \mathbf{x}_{t-1}^n, \mathbf{z}_t^n) \\ &\times p(\mathbf{z}_t^n | \mathbf{z}_{t-1}^n, \mathbf{x}_{t-1}^n, \mathbf{u}_{t-1}^n), \end{aligned} \quad (5)$$

and $p(\theta | \mathbf{h})$ is the factorized parameter prior

$$\begin{aligned} p(\theta | \mathbf{h}) &= p(\pi) \prod_{k=1}^K p(\mu_{1,k} | \Lambda_{1,k}) p(\Lambda_{1,k}) \\ &\times \prod_{k=1}^K p(\mathbf{A}_k | \Lambda_k) p(\mathbf{B}_k | \Lambda_k) p(\mathbf{c}_k | \Lambda_k) p(\Lambda_k) \\ &\times \prod_{k=1}^K p(\mathbf{K}_k | \Delta_k) p(\Delta_k) \prod_{i=1}^K p(\omega_{ik}). \end{aligned}$$

We choose all priors to be conjugate or semi-conjugate w.r.t. their likelihoods, if possible. Therefore, we place a normal-Wishart (NW) prior on the initial state distribution $(\mu_{1,k}, \Lambda_{1,k}) \sim \text{NW}(\mathbf{0}, \kappa_0, \Psi_0, \nu_0)$, and a matrix-normal-Wishart (MNW) on the linear transition dynamics $(\mathbf{A}_k, \mathbf{B}_k, \mathbf{c}_k, \Lambda_k) \sim \text{MNW}(\mathbf{0}, \mathbf{K}_0, \Phi_0, \rho_0)$. The initial discrete state takes a Dirichlet prior $\pi \sim \text{Dir}(\tau_0)$,

while the logistic transition parameters are governed by a non-conjugate zero-mean Gaussian with diagonal precision $\omega_{ik} \sim \mathcal{N}(\mathbf{0}, \alpha \mathbf{I})$. Finally, we place a separate matrix-normal-Wishart prior on the conditional action likelihood $(\mathbf{K}_k, \Delta_k) \sim \text{MNW}(\mathbf{0}, \mathbf{S}_0, \Gamma_0, \varepsilon_0)$. The quantities $(\kappa_0, \Psi_0, \nu_0, \mathbf{K}_0, \Phi_0, \rho_0, \tau_0, \alpha, \mathbf{S}_0, \Gamma_0, \varepsilon_0)$ are hyperparameters that we aggregate in the hyperparameter set \mathbf{h} .

The choice of priors is not restricted to these distributions. Depending on modeling assumptions, one can assume dynamics with diagonal noise matrices and pair them with gamma distribution priors. Moreover, if the system is known to have a state-independent noise process, the K Wishart and gamma priors can be *tied* across components, leading to a more structured representation.

B. Baum-Welch Expectation-Maximization

On closer examination of Equations (4) and (5), one can show that the optimization problem is non-convex with multiple local optima, since the complete-data likelihood $p(\mathcal{D}, \mathbf{Z}|\boldsymbol{\theta}) = p(\mathbf{X}, \mathbf{U}, \mathbf{Z}|\boldsymbol{\theta})$ can follow complex multi-modal densities. Another technical difficulty is the summation over all possible trajectories of the hidden variables \mathbf{Z}^n , which is of computational complexity $\mathcal{O}(NK^T)$ and is intractable in most cases. Expectation-maximization algorithms overcome the latter problem by introducing the variational posterior distribution over the hidden variables $q(\mathbf{Z}^n)$ and derive a lower bound on the complete log-probability function

$$\log \prod_{n=1}^N \sum_{\mathbf{z}^n} p(\mathcal{D}^n, \mathbf{Z}^n, \boldsymbol{\theta}) \geq \sum_{n=1}^N \sum_{\mathbf{z}^n} q(\mathbf{Z}^n) \log \frac{p(\mathcal{D}^n, \mathbf{Z}^n, \boldsymbol{\theta})}{q(\mathbf{Z}^n)}. \quad (6)$$

We can find a point estimate of the parameters $\boldsymbol{\theta}_{\text{MAP}}$ by following the standard scheme of EM, alternating between an expectation step (E-step), in which the lower bound in Equation (6) is maximized w.r.t. the variational distributions $q(\mathbf{Z}^n)$ given a parameter estimate $\hat{\boldsymbol{\theta}}$, a maximization step (M-step), that updates $\boldsymbol{\theta}$ given $(\hat{q}(\mathbf{Z}^n), \hat{\mathbf{h}})$, and finally an empirical Bayes step (EB-step) that updates \mathbf{h} given $\hat{q}(\mathbf{Z}^n)$ and $\hat{\boldsymbol{\theta}}$. A sketch of the iterative procedure is presented in Algorithm 1.

Algorithm 1: rARHMM Expectation-Maximization

```

input :  $K, \mathbf{X}, \mathbf{U}, \mathbf{h}$ 
initialize :  $\hat{\boldsymbol{\theta}} \sim p(\boldsymbol{\theta}|\mathbf{h}), \hat{\mathbf{h}} \leftarrow \mathbf{h}$ 
while  $\log p(\mathbf{X}, \mathbf{U}, \boldsymbol{\theta}|\mathbf{h})$  not converged do
  // Expectation step
  for  $n \leftarrow 1$  to  $N$  do
     $\alpha^n, \beta^n \leftarrow \text{forwardBackward}(\mathbf{X}^n, \mathbf{U}^n, \hat{\boldsymbol{\theta}})$ 
     $\gamma^n, \xi^n \leftarrow \text{smoothedPosteriors}(\alpha^n, \beta^n, \hat{\boldsymbol{\theta}})$ 
  end
  // Maximization step
   $\hat{\boldsymbol{\theta}} \leftarrow \text{maximize } Q(\hat{\boldsymbol{\theta}}, \gamma, \xi, \hat{\mathbf{h}})$ 
  // Empirical Bayes
   $\hat{\mathbf{h}} \leftarrow \hat{\mathbf{h}} + \varrho \nabla_{\mathbf{h}} Q(\mathbf{h}|\cdot)(\hat{\mathbf{h}})$ 
end
output :  $\hat{\boldsymbol{\theta}}$ 

```

1) *Exact Expectation Step*: Maximizing the lower bound w.r.t. $q(\mathbf{Z}^n)$ can be determined by reformulating Equation (6)

$$\begin{aligned} L &= \sum_{n=1}^N \sum_{\mathbf{z}^n} q(\mathbf{Z}^n) \log \frac{p(\mathbf{X}^n, \mathbf{Z}^n, \boldsymbol{\theta}|\mathbf{U}^n, \mathbf{h})}{q(\mathbf{Z}^n)} \\ &= \sum_{n=1}^N \log p(\mathbf{X}^n, \mathbf{U}^n, \boldsymbol{\theta}|\mathbf{h}) - \text{KL}(q(\mathbf{Z}^n) || p(\mathbf{Z}^n|\mathbf{X}^n, \mathbf{U}^n, \boldsymbol{\theta})). \end{aligned}$$

This form of the lower bound implies that the optimal variational distribution $\hat{q}(\mathbf{Z}^n)$ minimizes the Kullback-Leibler divergence, meaning

$$\hat{q}(\mathbf{Z}^n) = p(\mathbf{Z}^n|\mathbf{X}^n, \mathbf{U}^n, \boldsymbol{\theta}) = p(\mathbf{Z}^n|\mathbf{x}_{1:T}^n, \mathbf{u}_{1:T}^n, \boldsymbol{\theta}). \quad (7)$$

This update tightens the bound if the posterior model $\hat{q}(\mathbf{Z}^n)$ belongs to the same family of the true posterior [16]. Notice that the E-step is independent of the prior $p(\boldsymbol{\theta})$. Moreover, Equation (7) indicates that the E-step reduces to the computation of smoothed marginals $p(\mathbf{z}_t^n|\mathbf{x}_{1:T}^n, \mathbf{u}_{1:T}^n, \hat{\boldsymbol{\theta}})$ under the current parameter estimate $\hat{\boldsymbol{\theta}}$. Following [89] and [96], we derive a forward-backward algorithm, which enables closed-form, exact inference of these quantities

$$\begin{aligned} \gamma_t^n(k) &= p(\mathbf{z}_t^n = k | \mathbf{x}_{1:T}^n, \mathbf{u}_{1:T}^n) \\ &\propto p(\mathbf{z}_t^n = k | \mathbf{x}_{1:t}^n, \mathbf{u}_{1:t}^n) p(\mathbf{x}_{t+1:T}^n, \mathbf{u}_{t+1:T}^n | \mathbf{z}_t^n = k, \mathbf{x}_t^n, \mathbf{u}_t^n) \\ &= \alpha_t^n(k) \beta_t^n(k), \end{aligned}$$

where $\alpha_t^n(k) = p(\mathbf{z}_t^n = k | \mathbf{x}_{1:t}^n, \mathbf{u}_{1:t}^n)$ is the message which computes the filtered marginals via a forward recursion

$$\begin{aligned} \alpha_t^n(k) &\propto p(\mathbf{x}_t^n | \mathbf{x}_{t-1}^n, \mathbf{u}_{t-1}^n, \mathbf{z}_t^n = k) p(\mathbf{u}_t^n | \mathbf{x}_t^n, \mathbf{z}_t^n = k) \\ &\quad \times \sum_{j=1}^K p(\mathbf{z}_t^n = k | \mathbf{z}_{t-1}^n = j, \mathbf{x}_{t-1}^n, \mathbf{u}_{t-1}^n) \alpha_{t-1}^n(j), \end{aligned}$$

and $\beta_t^n(k) = p(\mathbf{x}_{t+1:T}^n | \mathbf{z}_t^n = k, \mathbf{x}_t^n, \mathbf{u}_t^n)$ is the backward message that performs smoothing by computing the conditional likelihood of future evidence

$$\begin{aligned} \beta_t^n(k) &= \sum_{j=1}^K \beta_{t+1}^n(j) p(\mathbf{z}_{t+1}^n = j | \mathbf{z}_t^n = k, \mathbf{x}_t^n, \mathbf{u}_t^n) \\ &\quad \times p(\mathbf{x}_{t+1}^n | \mathbf{x}_t^n, \mathbf{u}_t^n, \mathbf{z}_{t+1}^n = j) p(\mathbf{u}_{t+1}^n | \mathbf{x}_{t+1}^n, \mathbf{z}_{t+1}^n = j). \end{aligned}$$

Additionally, by combining both forward and backward messages, we can compute the two-slice smoothed marginals $p(\mathbf{z}_t^n, \mathbf{z}_{t+1}^n | \mathbf{x}_{1:T}^n, \mathbf{u}_{1:T}^n, \hat{\boldsymbol{\theta}})$ which will be useful during the maximization and empirical Bayes steps

$$\begin{aligned} \xi_{t,t+1}^n(i, j) &= p(\mathbf{z}_t^n = i, \mathbf{z}_{t+1}^n = j | \mathbf{x}_{1:T}^n, \mathbf{u}_{1:T}^n) \\ &\propto p(\mathbf{x}_{t+1}^n | \mathbf{x}_t^n, \mathbf{u}_t^n, \mathbf{z}_{t+1}^n = j) p(\mathbf{u}_{t+1}^n | \mathbf{x}_{t+1}^n, \mathbf{z}_{t+1}^n = j) \\ &\quad \times \alpha_t^n(i) p(\mathbf{z}_{t+1}^n = j | \mathbf{z}_t^n = i, \mathbf{x}_t^n, \mathbf{u}_t^n) \beta_{t+1}^n(j), \end{aligned}$$

This concludes all needed computations for the forward-backward messages of the E-step.

2) *Stochastic Maximization Step*: After performing the E-step and computing the smoothed posteriors, we are able to evaluate the lower bound and maximize it w.r.t. $\boldsymbol{\theta}$ given $(\hat{q}(\mathbf{Z}^n), \hat{\mathbf{h}})$. By plugging Equation (7) into (6) and leveraging

conditional independence between the rARHMM components, we arrive at the complete log-probability function

$$\begin{aligned}
Q &= \sum_{n=1}^N \sum_{\mathbf{z}^n} \hat{q}(\mathbf{Z}^n) \log p(\mathbf{X}^n, \mathbf{U}^n, \mathbf{Z}^n, \boldsymbol{\theta} | \hat{\mathbf{h}}) \\
&= \log p(\boldsymbol{\theta} | \hat{\mathbf{h}}) + \sum_{k=1}^K \sum_{n=1}^N \gamma_1^n \left[\log \pi_k + \log N(\mathbf{x}_1^n | \boldsymbol{\mu}_{1,k}, \boldsymbol{\Lambda}_{1,k}) \right] \\
&\quad + \sum_{k=1}^K \sum_{n=1}^N \sum_{t=2}^T \gamma_t^n \log N(\mathbf{x}_t^n | \mathbf{A}_k \mathbf{x}_{t-1}^n + \mathbf{B}_k \mathbf{u}_{t-1}^n + \mathbf{c}_k, \boldsymbol{\Lambda}_k) \\
&\quad + \sum_{k=1}^K \sum_{n=1}^N \sum_{t=1}^T \gamma_t^n \log N(\mathbf{u}_t^n | \mathbf{K}_k \phi(\mathbf{x}_{t-1}^n), \boldsymbol{\Delta}_k) \\
&\quad + \sum_{i=1}^K \sum_{j=1}^K \sum_{n=1}^N \sum_{t=2}^T \xi_{t-1,t}^n \log \chi_{ij}(\mathbf{x}_{t-1}^n, \mathbf{u}_{t-1}^n, \boldsymbol{\omega}_{ij}).
\end{aligned}$$

The optimization of Q is commonly done via coordinate ascent. Simpler models, e.g. Gaussian- and Binomial-HMMs, lead to an exact, convex M-step with closed-form optimality conditions. This is not the case in rARHMM, given the possibility of choosing nonlinear transition predictor functions. Such a choice leads to an approximate, non-convex M-step that requires gradient-based updates. In such cases, stochastic optimization is advisable [97], since batched noisy gradient estimates allow algorithms to escape shallow local minima and reduce the computational load that comes with evaluating the gradients for all data instances.

Consequently, in our implementation of the M-step, we apply stochastic optimization on the transition parameters $\boldsymbol{\omega}$. We use a stochastic gradient ascent direction with an adaptive learning rate ε and batch size M [97]

$$\begin{aligned}
\boldsymbol{\omega}^{(l+1)} &= \boldsymbol{\omega}^l + \frac{\varepsilon}{M} \sum_{m=1}^M \nabla_{\boldsymbol{\omega}} Q_m(\boldsymbol{\omega}^l), \\
\nabla_{\boldsymbol{\omega}} Q_m &= \nabla_{\boldsymbol{\omega}} \left[\log p(\boldsymbol{\omega} | \alpha) + \sum_{i=1}^K \sum_{j=1}^K \xi_m \log \chi_{ij}(\mathbf{x}_m, \mathbf{u}_m, \boldsymbol{\omega}_{ij}) \right].
\end{aligned}$$

For the parameters with conjugate priors, we derive closed-form optimality conditions. Effectively, this part of the optimization constitutes formulating the posterior distribution of all remaining parameters and taking the mode of each posterior density for a point estimate update. By considering only relevant terms, we reformulate the optimization of the initial gating parameter $\boldsymbol{\pi}$ as

$$\max_{\boldsymbol{\pi}} \log \text{Dir}(\boldsymbol{\pi} | \hat{\boldsymbol{\tau}}_0) + \sum_{k=1}^K \sum_{n=1}^N \gamma_1^n \log \pi_k,$$

while the objective of the initial state parameters $(\boldsymbol{\mu}_{1,k}, \boldsymbol{\Lambda}_{1,k})$ can be decoupled for each k as follows

$$\begin{aligned}
\max_{\boldsymbol{\mu}, \boldsymbol{\Lambda}} \log \text{NW}(\boldsymbol{\mu}_{1,k}, \boldsymbol{\Lambda}_{1,k} | (\mathbf{0}, \hat{\boldsymbol{\kappa}}_0, \hat{\boldsymbol{\Psi}}_0, \hat{\nu}_0)_k) \\
+ \sum_{n=1}^N \gamma_1^n \log N(\mathbf{x}_1^n | \boldsymbol{\mu}_{1,k}, \boldsymbol{\Lambda}_{1,k}).
\end{aligned}$$

Analogously, the objective terms related to the dynamics parameter $(\mathbf{A}_k, \mathbf{B}_k, \mathbf{c}_k, \boldsymbol{\Lambda}_k)$ are also decoupled to k parts

$$\begin{aligned}
\max_{\mathbf{A}, \mathbf{B}, \mathbf{c}, \boldsymbol{\Lambda}} \log \text{MNW}(\mathbf{A}_k, \mathbf{B}_k, \mathbf{c}_k, \boldsymbol{\Lambda}_k | (\mathbf{0}, \hat{\mathbf{K}}_0, \hat{\boldsymbol{\Phi}}_0, \hat{\nu}_0)_k) \\
+ \sum_{n=1}^N \sum_{t=2}^T \gamma_t^n \log N(\mathbf{x}_t^n | \mathbf{A}_k \mathbf{x}_{t-1}^n + \mathbf{B}_k \mathbf{u}_{t-1}^n + \mathbf{c}_k, \boldsymbol{\Lambda}_k),
\end{aligned}$$

and, similarly, the controller parameters $(\mathbf{K}_k, \boldsymbol{\Delta}_k)$

$$\begin{aligned}
\max_{\mathbf{K}, \boldsymbol{\Delta}} \log \text{MNW}(\mathbf{K}_k, \boldsymbol{\Delta}_k | (\mathbf{0}, \hat{\mathbf{S}}_0, \hat{\boldsymbol{\Gamma}}_0, \hat{\nu}_0)_k) \\
+ \sum_{n=1}^N \sum_{t=1}^T \gamma_t^n \log N(\mathbf{u}_t^n | \mathbf{K}_k \phi(\mathbf{x}_t^n), \boldsymbol{\Delta}_k).
\end{aligned}$$

Due to space constraints, we will refrain from stating the explicit solution for these former problems. Instead, we provide a general outline of how to compute these posteriors and their modes in Appendix I and II.

3) Approximate Empirical Bayes: Approach that leverage data-independent assumptions run the risk of prior misspecification. In the MAP approach we present, the priors are weakly informative and carry little information. Their main purpose is to regularize greedy updates that might lead to premature convergence. However, when there is little data, the priors, especially those on the precision matrices⁴, may dominate the posterior probability, leading to an over-regularization under-fitting of the objective. Empirical Bayes approaches remedy this issue by integrating out the parameters $\boldsymbol{\theta}$ and optimizing the marginal likelihood w.r.t. the hyperparameters \mathbf{h} [95]. In our setting, marginalizing all hidden quantities does not admit a closed-form formula. An approximate approach to empirical Bayes is to interleave the E- and M-steps with hyperparameter updates that optimize the lower bound given an estimate of parameters $\hat{\boldsymbol{\theta}}$ and a step size ϱ

$$\begin{aligned}
\mathbf{h}^{(l+1)} &= \mathbf{h}^{(l)} + \varrho \nabla_{\mathbf{h}} Q(\mathbf{h}^l | \cdot), \\
\nabla_{\mathbf{h}} Q &= \nabla_{\mathbf{h}} \left[\log p(\hat{\boldsymbol{\theta}} | \mathbf{h}) \right].
\end{aligned}$$

The necessary gradients for performing the empirical Bayes updates are provided in Appendix II.

C. Importance Weighting

The previous sections sketched the outline of a MAP approach for inferring the parameters of an rARHMM given an observed data distribution $p(\mathbf{X}, \mathbf{U})$. In order to fulfill the policy improvement updates mentioned in Section V-E, the EM objective in Equation (4) has to be augmented with importance weights from Equation (2). This augmentation only influences the maximization and empirical Bayes steps by multiplying the smoothed posteriors γ_t^n and $\xi_{t,t+1}^n$ with the importance weights $w_t^n = \exp[A(\mathbf{x}_t^n, \mathbf{u}_t^n, \mathbf{z}_t^n)/\eta]$.

VII. EMPIRICAL EVALUATION

In this section, we evaluate benchmarks related to the inference of rARHMMs and learning hybrid controllers via Hb-REPS. First, to validate the choice of this representation

⁴See [98] for a discussion on the choice of non-informative precision priors.

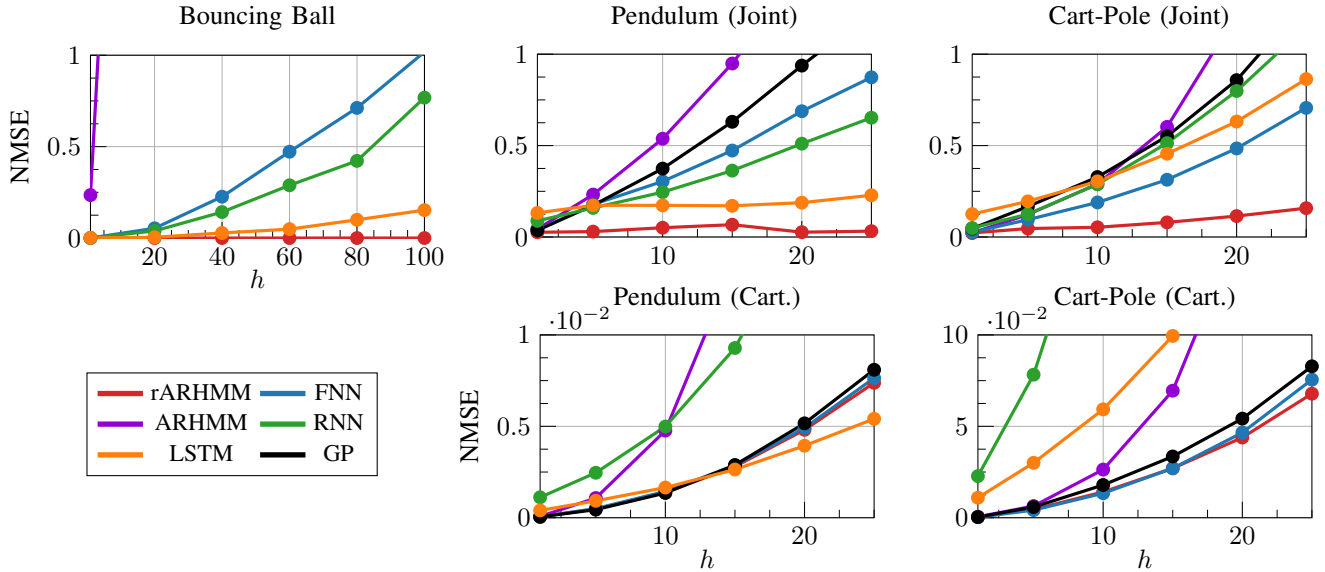


Fig. 3: System identification: Comparing the h -step NMSE of rARHMMs to other popular dynamics approximation models. Every evaluation point is averaged over 24 data splits. Benchmarking on three dynamical systems, a bouncing ball, a pendulum and a cart-pole. In this limited-data scenario, rARHMM exhibit the most consistent approximation capabilities.

	Bouncing Ball	Pendulum (Joint)	Pendulum (Cartesian)	Cart-Pole (Joint)	Cart-Pole (Cartesian)
ARHMM	22 (2)	180 (9)	130 (5)	287 (7)	275 (5)
rARHMM	86 (2)	468 (9)	582 (9)	575 (7)	711 (7)
FNN	1250 (32)	546 (64)	1315 (32)	1380 (32)	1445 (32)
RNN	12866 (64)	50306 (128)	3427 (32)	50820 (128)	51077 (128)
LSTM	200450 (128)	51074 (64)	51395 (64)	201732 (128)	202373 (128)

TABLE I: System identification: Qualitative comparison of model complexity for the best performing representations in Figure 3. The values reflect the total number of parameters of each model. The values in parentheses represent the hidden layer sizes S of the neural models and the number of discrete components K for the (r)ARHMM, respectively.

of hybrid dynamics, we assess the performance of rARHMM in an open-loop setting. Second, we test the closed-loop rARHMM and its ability to capture and decompose an expert nonlinear controller in an imitation learning scenario. Finally, we use rARHMMs in the proposed RL algorithm Hb-REPS to iteratively solve the infinite horizon stochastic control objective and optimize piecewise locally polynomial controllers and value functions. Here we make no claim to the absolute efficiency of our approach when compared to other state-of-the-art algorithms. Instead, we aim to provide an empirical proof-of-work that supports further research into sample-based hybrid system optimization as a framework for structured nonlinear control.

A. System Identification Examples

We empirically benchmark rARHMMs on nonlinear systems. We aim to quantify the quality of learned open-loop models and their ability to capture the underlying dynamics. For this purpose, we set up a direct comparison to popular representations in a *long-horizon* and *limited-data* setting.⁵

In this evaluation, we focus on rARHMMs with exogenous inputs. We aim to learn the dynamics of three simulated de-

terministic systems; a bouncing ball, an actuation-constrained pendulum, and a cart-pole system. We compare the predictive power of rARHMMs to classical non-recurrent autoregressive hidden Markov models (ARHMMs) [17], feed-forward neural nets (FNNs), Gaussian processes (GPs)⁶, long-short-term memory networks (LSTMs) [99] and recurrent neural networks (RNNs). During the evaluation, we collect segregated training and test datasets. The training dataset is randomly split into 24 groups, each containing a subset of trajectories, and used to train different instances of all representations. These instances are then tested on the test dataset. All neural models have 2 hidden layers, which we test for a variety of different layer sizes, $S = \{16, 32, 64, 128, 256, 512\}$ for FNNs, $S = \{16, 32, 64, 128, 256\}$ for RNNs, and $S = \{16, 32, 64, 128\}$ for LSTMs. In the case of (r)ARHMMs, we test with different component sizes K , dependent on the task. As a metric, we evaluate the normalized mean square error (NMSE), averaged over the 24 data splits for a range of horizons. During the evaluation, we comb through the test trajectories step by step and predict the given horizon. Moreover, in Table I, we qualitatively compare the complexity of all representations in terms of their total number of parameters.

⁵Public code base available on <https://github.com/hanyas/sds>.

⁶With an RBF kernel and hyperparameter optimization

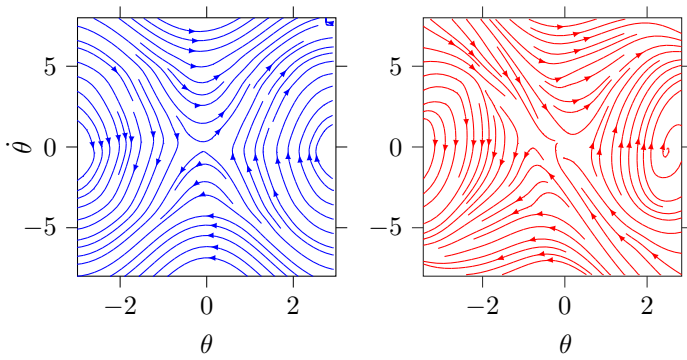


Fig. 4: Imitation learning: Phase space of the pendulum. The identified unforced dynamics is on the left (blue). The learned model qualitatively captures the iconic phase portrait. On the right (red), the closed-loop dynamics. The learned stationary hybrid policy with 5 regions successfully imitates a global nonlinear soft actor-critic (SAC) controller to stabilize the system around the origin.

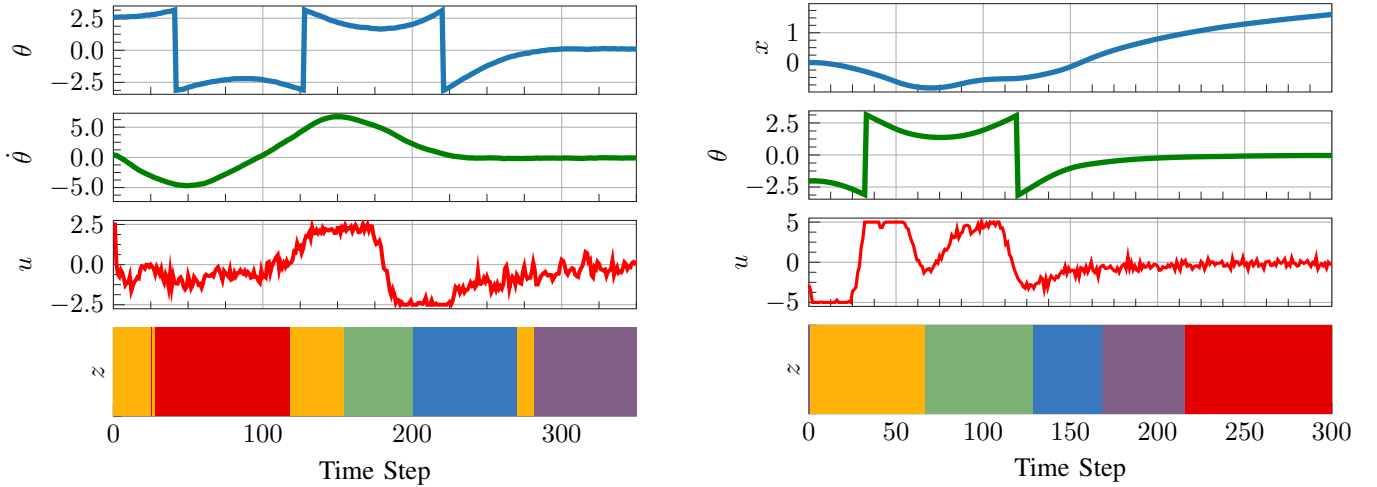


Fig. 5: Imitation learning: Sample trajectories from the learned stationary hybrid policies on the pendulum (left) and cart-pole (right) environments. Both hybrid controllers are able to consistently solve both tasks, while relying on simple local representations of the feedback controllers. The colors indicate active dynamics and control at the respective time steps.

a) Bouncing Ball: This example is a canonical instance of a dual-regime hybrid dynamical system because of the hard velocity switch at the moment of impact. We simulate the dynamics with a frequency of 20 Hz and collect 25 training trajectories with different initial heights and velocities, each 30 s long. This dataset is split 24 folds with ten trajectories, 10×150 data points, in each subset. The test dataset consists of 5 trajectories, each 30 s long. We evaluate the NMSE for horizons $h = \{1, 20, 40, 60, 80\}$ time steps. We did not evaluate a GP model in this setting due to the long prediction horizons that result in a very high computation effort during evaluation time. The (r)ARHMMs are tested for $K = 2$. The logistic link function of an rARHMM is parameterized by a neural net with one hidden layer containing 16 neurons. The results in Figure 3 show that the rARHMM can approximate the true dynamics very well and outperforms the standard ARHMMs and all other neural models.

b) Pendulum and Cart-Pole: These two systems are classical benchmarks from the control literature. Here we consider two different observation models, one in the wrapped joint space, where the angle $\theta \in [-\pi, \pi]$ includes a sharp discontinuity, and a second model with smooth observations that parameterize the angle with the Cartesian trigonometric features $\{\cos(\theta), \sin(\theta)\}$. Both dynamics are simulated with a frequency of 100 Hz. We collect 25 training trajectories starting from different initial conditions and applying random

uniform explorative actions. Each trajectory is 2.5 s long. The 24 splits consist of 10 trajectories each, 10×250 data points. The test dataset consists of 5 trajectories, each 2.5 s long. Forecasting accuracy is evaluated for horizons $h = \{1, 5, 10, 15, 20, 25\}$. The (r)ARHMMs are tested for $K = \{3, 5, 7, 9\}$ on both tasks. The logistic link function of the rARHMM is parameterized by a neural net with one hidden layer containing 24 neurons. The forecast evaluation, as shown in Figure 3, provides empirical evidence for the representation power of rARHMMs in both smooth and discontinuous state spaces. FNNs and GPs perform equally well in the smooth Cartesian observation space, struggle, however, in the discontinuous space, similar to RNNs and LSTMs.

B. Closed-Loop Imitation Learning

Before applying the RL method proposed in Section V-A, we first want to analyze the closed-loop rARHMM with endogenous inputs as an imitation learning framework. The task is to reproduce the closed-loop behavior of expert policies on challenging nonlinear systems. For this purpose, we train two different feedback experts on the pendulum and cart-pole. The two environments are simulated at 50 Hz and are influenced by static Gaussian noise with a standard deviation $\sigma = 1 \times 10^{-2}$. The experts are two-layer neural nets with 4545 parameters (pendulum) and 17537 parameters (cart-pole), optimized with the soft actor-critic (SAC) algorithm [9].

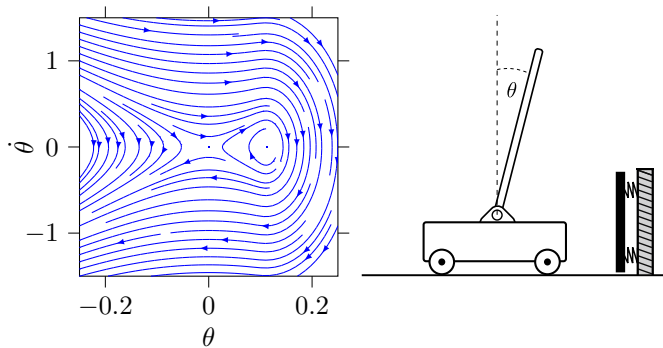


Fig. 6: Cart-pole with elastic wall: a hybrid system with two linear regimes. The cart-pole is linearized around the upright position, while the wall is elastic and modeled by a spring. The switching boundary is linear. The unforced dynamics is depicted on the left (blue) and the aim is to stabilize the pole around the origin.

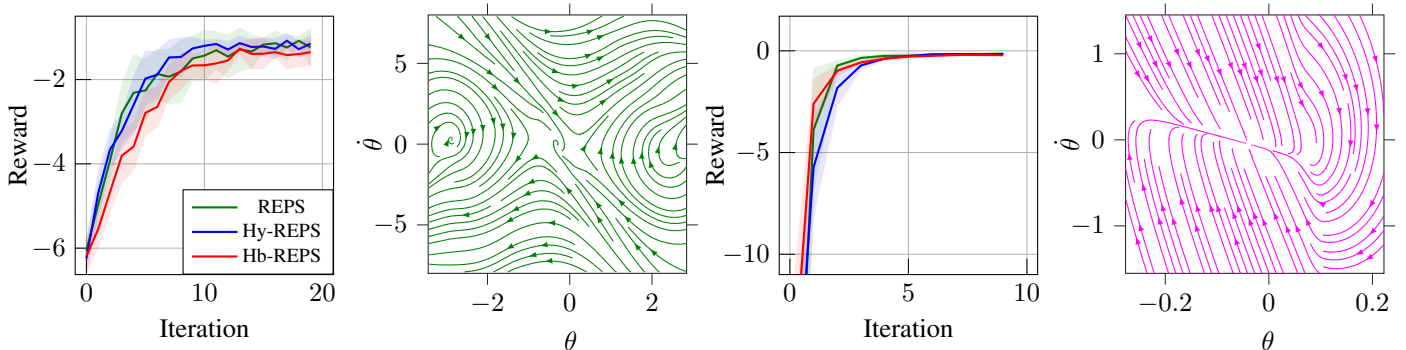


Fig. 7: Reinforcement learning: REPS, Hy-REPS and Hb-REPS evaluated on the pendulum swing-up (left) and cart-pole stabilization (right) tasks. By inspecting the learning curves, mean reward with 95% confidence, we conclude that all algorithms perform equally well in terms of transient and final performance. However, Hb-REPS relies on simpler polynomial models of the policy and value function, while Hy-REPS and REPS rely on nonlinear representations. The phase portraits depict the closed-loop behavior achieved by Hb-REPS. Hb-REPS solves both tasks and stabilizes the systems around the origin.

For imitation, we construct two 5-regime rARHMMs with locally polynomial policies of the third order. The hybrid controllers have a total number of parameters of 100 (pendulum) and 280 (cart-pole). Imitation is realized on a dataset of 25 trajectories, each 5 s long, for each environment and using the EM technique from Section VI while setting the importance weights to 1. The decomposed controllers complete the task of swinging up and stabilizing both systems with over 95% success rate. Figure 4 shows the phase portraits of the unforced dynamics and closed-loop control identified during imitation. Figure 5 depicts sampled trajectories of the hybrid policies highlighting the switching behavior.

C. Hybrid Reinforcement Learning

Finally, by bringing all previous concepts together, we evaluate the qualitative performance of the proposed hybrid policy search algorithm Hb-REPS on two nonlinear stochastic dynamical systems: an underpowered pendulum swing-up and a cart-pole stabilization task that explicitly simulates an abrupt switch in dynamics when the cart hits an elastic wall.

We compare the performance of Hb-REPS to two baselines. The first is a *vanilla* version of REPS that does not maintain any hierarchical structure and uses nonlinear function approximators with random Fourier features (RFFs) [100] to represent both policy and value function. The second baseline assumes a hierarchical policy structure and a nonlinear value function with Fourier features. This baseline is akin to what is implemented in [67], albeit with a hierarchy based on state abstraction rather than time. We will refer to this algorithm

version as hierarchical REPS (Hy-REPS). We assume an offline learning phase in which the hybrid models are learned from pre-collected data.

a) Pendulum Swing-up: In this experiment, the power-limited pendulum is simulated at 50 Hz and perturbed by Gaussian noise with a standard deviation $\sigma = 1 \times 10^{-2}$. The REPS agent relies on a policy and value function with 50 and 75 Fourier features, respectively. Hy-REPS assumes a similar form of the value function but with five third-order polynomial policies. Hb-REPS represents both policy and value function with five third-order polynomials. Empirical results in Figure 7 (left half) feature comparable learning performance of all algorithms over ten random seeds. Every iteration involves 5000 interactions with the environment. We provide a phase portrait of the closed-loop behavior for a qualitative assessment of the final hybrid policy.

b) Cart-pole Stabilization: This evaluation features a cart-pole constrained by an elastic wall modeled as a spring. The dynamics are linearized around the upright position, naturally resulting in a two-regime hybrid system. The environment is simulated at 100 Hz and perturbed by Gaussian noise with a standard deviation $\sigma = 1 \times 10^{-4}$. The REPS policy and value function both use 25 random Fourier features. Hy-REPS adopts the same value function structure with two affine linear policies. Hb-REPS also assumes two affine linear policies combined with two second-order local value functions. The results in Figure 7 (right half) depict matching learning performance of the three approaches over ten random seeds. Every iteration involves 2500 interactions with the environment.

VIII. DISCUSSION

We presented a data-driven view of hybrid systems as an alternative paradigm to common hybrid control techniques that rely on trajectory optimization and model predictive control. However, our approach is not restricted to the class of explicit hybrid dynamics and can be seen as a general approach to structured nonlinear control. We argue that this structure often exists under the hood of complex neural representation. Therefore, making it explicit may offer an avenue to apply Occam's razor and regularize over-parameterized representations. Initial empirical results support this motivation. The proposed hybrid reinforcement learning technique can do without neural networks and instead rely on a hierarchy of local polynomial representations dictated by a hybrid model structure.

Nonetheless, the application of this work is limited to simple lower-dimensional systems. In our opinion, the inference techniques used in this paper, although a viable alternative to expensive mixed-integer optimization, still present a big bottleneck in the face of scalability to more complex systems and higher dimensions. While our MAP approach significantly improves the quality of expectation-maximization solutions, it nevertheless struggles in more challenging environments.

A possible course of action is to investigate Bayesian non-parametric extensions of hybrid dynamic Bayesian networks based on non-conjugate variational inference. Fully Bayesian methods tend to improve learning in large structured models significantly. Another potential avenue of research is to improve the hybrid reinforcement learning framework by considering the control-as-inference paradigm. Such approaches may offer ways of integrating the Bayesian structure of the models into the control optimization and, in the process, achieve an uncertainty-aware approach that is better equipped to deal with the exploration-exploitation dilemma.

APPENDIX I EXPONENTIAL FAMILY

The upcoming chapters mainly consider random variables with probability density functions belonging to the exponential family. The unified minimal parameterization of this class of distributions lends itself for convenient and efficient posterior computation when paired with conjugate priors.

We assume the natural form for a probability density of a random variable \mathbf{x}

$$f(\mathbf{x}|\boldsymbol{\eta}) = h(\mathbf{x}) \exp [\boldsymbol{\eta} \cdot \mathbf{t}(\mathbf{x}) - a(\boldsymbol{\eta})],$$

where $h(\mathbf{x})$ is the base measure, $\boldsymbol{\eta}$ are the natural parameters, $\mathbf{t}(\mathbf{x})$ are the sufficient statistics and $a(\boldsymbol{\eta})$ is the log-partition function, or log-normalizer. Following the same notation, a conjugate prior $g(\boldsymbol{\eta}|\boldsymbol{\alpha})$ to the likelihood $f(\mathbf{x}|\boldsymbol{\eta})$ has the form

$$g(\boldsymbol{\eta}|\boldsymbol{\lambda}) = h(\boldsymbol{\eta}) \exp [\boldsymbol{\lambda} \cdot \mathbf{t}(\boldsymbol{\eta}) - a(\boldsymbol{\lambda})],$$

with prior sufficient statistics $\mathbf{t}(\boldsymbol{\eta}) = [\boldsymbol{\eta}, -a(\boldsymbol{\eta})]^\top$ and hyperparameters $\boldsymbol{\lambda} = [\boldsymbol{\alpha}, \boldsymbol{\beta}]^\top$. By applying Bayes' rule, we can directly infer the posterior $q(\boldsymbol{\eta}|\mathbf{x})$

$$q(\boldsymbol{\eta}|\mathbf{x}) \propto f(\mathbf{x}|\boldsymbol{\eta})g(\boldsymbol{\eta}|\boldsymbol{\lambda}) \\ \propto \exp [\boldsymbol{\rho}(\mathbf{x}, \boldsymbol{\lambda}) \cdot \mathbf{t}(\boldsymbol{\eta}) - a(\boldsymbol{\rho})],$$

where the posterior natural parameters $\boldsymbol{\rho}(\mathbf{x}, \boldsymbol{\lambda})$ are a function of the likelihood sufficient statistics $\mathbf{t}(\mathbf{x})$ and prior hyperparameters $[\boldsymbol{\alpha}, \boldsymbol{\beta}]$

$$\boldsymbol{\rho}(\mathbf{x}, \boldsymbol{\lambda}) = [\boldsymbol{\alpha} + \mathbf{t}(\mathbf{x}), \boldsymbol{\beta} + \mathbf{1}]^\top.$$

The structure of the resulting posterior reveals a simple recipe for data-driven inference. By moving into the natural space, the posterior parameters are computed by combining the prior hyperparameters with the likelihood sufficient statistics and log-partition function. By definition, every exponential family distribution has a minimal natural parameterization that leads to a unique decomposition of these quantities [101].

APPENDIX II CONJUGATE POSTERiors

We present an outline of all M-step and empirical Bayes updates. We use an adapted form of the exponential natural parameterization, as it offers a clear methodology on how to derive and implement such updates for all distributions.

A. Categorical with Dirichlet Prior

A weighted categorical likelihood over a one-hot random variable \mathbf{z} with size K has the form

$$p(\mathbf{Z}|\boldsymbol{\pi}) = \prod_{n=1}^N \text{Cat}(\mathbf{z}_n|\boldsymbol{\pi})^{w_n} \\ \propto \exp \left\{ \begin{bmatrix} \log \pi_1 \\ \vdots \\ \log \pi_K \end{bmatrix} \cdot \begin{bmatrix} \sum_{n=1}^N w_{n,1} \\ \vdots \\ \sum_{n=1}^N w_{n,K} \end{bmatrix} \right\},$$

where w_{nk} are the importance weights for each category K . The conjugate prior is a Dirichlet $p(\boldsymbol{\pi})$ distribution

$$p(\boldsymbol{\pi}) = \text{Dir}(\boldsymbol{\pi}|\boldsymbol{\tau}_0) \\ \propto \exp \left\{ \begin{bmatrix} \tau_{0,1} - 1 \\ \vdots \\ \tau_{0,K} - 1 \end{bmatrix} \cdot \begin{bmatrix} \log \pi_1 \\ \vdots \\ \log \pi_K \end{bmatrix} \right\},$$

The posterior $q(\boldsymbol{\pi})$ is likewise a Dirichlet distribution

$$q(\boldsymbol{\pi}) = \text{Dir}(\boldsymbol{\pi}|\boldsymbol{\tau}) \\ \propto \exp \left\{ \begin{bmatrix} \tau_{0,1} - 1 + \sum_{n=1}^N w_{n,1} \\ \vdots \\ \tau_{0,K} - 1 + \sum_{n=1}^N w_{n,K} \end{bmatrix} \cdot \begin{bmatrix} \log \pi_1 \\ \vdots \\ \log \pi_K \end{bmatrix} \right\}.$$

The maximization step requires computing the mode categorical weights. For a Dirichlet distribution the mode weights are $\hat{\boldsymbol{\pi}} = (\boldsymbol{\tau} - 1) / (\sum_{k=1}^K \tau_k - K)$ with $\tau_k > 1$. The parameter vector $\boldsymbol{\tau}$ is given by

$$\tau_k = \tau_{0,k} + \sum_{n=1}^N w_{n,k} \quad \forall k \in [1, K].$$

Finally, the gradients of prior parameters needed during the empirical Bayes incremental updates are

$$\frac{\partial \log p(\boldsymbol{\pi})}{\partial \tau_k} = \psi(\sum_{k=1}^K \tau_k) - \psi(\tau_k) + \log \pi_k,$$

where ψ stands for the digamma function.

B. Gaussian with Normal-Wishart Prior

A weighted Gaussian likelihood over a random variable $\mathbf{x} \in \mathbb{R}^d$ has the following precision-based parameterization

$$p(\mathbf{X}|\boldsymbol{\mu}, \boldsymbol{\Lambda}) = \prod_{n=1}^N N(\mathbf{x}_n|\boldsymbol{\mu}, \boldsymbol{\Lambda})^{w_n} \\ \propto \exp \left\{ \begin{bmatrix} \boldsymbol{\Lambda}\boldsymbol{\mu} \\ \boldsymbol{\mu}^\top \boldsymbol{\Lambda}\boldsymbol{\mu} \\ \boldsymbol{\Lambda} \\ \log |\boldsymbol{\Lambda}| \end{bmatrix} \cdot \begin{bmatrix} \sum_{n=1}^N w_n \mathbf{x}_n \\ -\frac{1}{2} \sum_{n=1}^N w_n \\ -\frac{1}{2} \sum_{n=1}^N w_n \mathbf{x}_n \mathbf{x}_n^\top \\ \frac{1}{2} \sum_{n=1}^N w_n \end{bmatrix} \right\},$$

where w_n are the importance weights. The conjugate prior $p(\boldsymbol{\mu}, \boldsymbol{\Lambda})$ is a normal-Wishart distribution with zero mean

$$p(\boldsymbol{\mu}, \boldsymbol{\Lambda}) = N(\boldsymbol{\mu}|\mathbf{0}, \kappa_0 \boldsymbol{\Lambda}) W(\boldsymbol{\Lambda}|\boldsymbol{\Psi}_0, \nu_0) \\ \propto \exp \left\{ \begin{bmatrix} \mathbf{0} \\ -\frac{1}{2} \kappa_0 \\ -\frac{1}{2} \boldsymbol{\Psi}_0^{-1} \\ \frac{1}{2}(\nu_0 - d) \end{bmatrix} \cdot \begin{bmatrix} \boldsymbol{\Lambda}\boldsymbol{\mu} \\ \boldsymbol{\mu}^\top \boldsymbol{\Lambda}\boldsymbol{\mu} \\ \boldsymbol{\Lambda} \\ \log |\boldsymbol{\Lambda}| \end{bmatrix} \right\}.$$

The resulting posterior $q(\boldsymbol{\mu}, \boldsymbol{\Lambda})$ is also a normal-Wishart

$$q(\boldsymbol{\mu}, \boldsymbol{\Lambda}) = N(\boldsymbol{\mu}|\mathbf{m}, \kappa \boldsymbol{\Lambda}) W(\boldsymbol{\Lambda}|\boldsymbol{\Psi}, \nu) \\ \propto \exp \left\{ \begin{bmatrix} \sum_{n=1}^N w_n \mathbf{x}_n \\ -\frac{1}{2}(\kappa_0 + \sum_{n=1}^N w_n) \\ -\frac{1}{2}(\boldsymbol{\Psi}_0^{-1} + \sum_{n=1}^N w_n \mathbf{x}_n \mathbf{x}_n^\top) \\ \frac{1}{2}(\nu_0 - d + \sum_{n=1}^N w_n) \end{bmatrix} \cdot \begin{bmatrix} \boldsymbol{\Lambda}\boldsymbol{\mu} \\ \boldsymbol{\mu}^\top \boldsymbol{\Lambda}\boldsymbol{\mu} \\ \boldsymbol{\Lambda} \\ \log |\boldsymbol{\Lambda}| \end{bmatrix} \right\}.$$

The vector and matrix modes of a normal-Wishart distribution are $\hat{\boldsymbol{\mu}} = \mathbf{m}$ and $\hat{\boldsymbol{\Lambda}} = (\nu - d)\boldsymbol{\Psi}$, respectively. The posterior parameters needed to determine the modes are

$$\kappa = \kappa_0 + \sum_{n=1}^N w_n, \\ \mathbf{m} = 1/\kappa \sum_{n=1}^N w_n \mathbf{x}_n, \\ \nu = \nu_0 + \sum_{n=1}^N w_n, \\ \boldsymbol{\Psi} = (\boldsymbol{\Psi}_0^{-1} + \sum_{n=1}^N w_n \mathbf{x}_n \mathbf{x}_n^\top - \kappa \mathbf{m} \mathbf{m}^\top)^{-1}.$$

The gradients required in empirical Bayes are

$$\frac{\partial \log p(\boldsymbol{\mu}, \boldsymbol{\Lambda})}{\partial \kappa_0} = \frac{d}{2} \frac{1}{\kappa_0} - \frac{1}{2} \boldsymbol{\mu}^\top \boldsymbol{\Lambda}\boldsymbol{\mu}, \\ \frac{\partial \log p(\boldsymbol{\mu}, \boldsymbol{\Lambda})}{\partial \boldsymbol{\Psi}_0} = \frac{1}{2} (\boldsymbol{\Psi}_0^{-1} \boldsymbol{\Lambda} \boldsymbol{\Psi}_0^{-1})^\top - \frac{\nu_0}{2} (\boldsymbol{\Psi}_0^{-1})^\top, \\ \frac{\partial \log p(\boldsymbol{\mu}, \boldsymbol{\Lambda})}{\partial \nu_0} = \frac{1}{2} (\log |\boldsymbol{\Lambda}| - d \log(2) - \log |\boldsymbol{\Psi}| - \psi(\frac{\nu_0}{2})).$$

C. Linear-Gaussian with Matrix-Normal-Wishart Prior

A weighted linear-Gaussian likelihood takes a random input variable $\mathbf{x} \in \mathbb{R}^d$ and returns a response random variable $\mathbf{y} \in \mathbb{R}^m$ according to a linear mapping $\mathbf{A} : \mathbb{R}^d \rightarrow \mathbb{R}^m$

$$p(\mathbf{Y}|\mathbf{X}, \mathbf{A}, \mathbf{V}) = \prod_{n=1}^N N(\mathbf{y}_n|\mathbf{x}_n, \mathbf{A}, \mathbf{V})^{w_n} \\ \propto \exp \left\{ \begin{bmatrix} \mathbf{V}\mathbf{A} \\ \mathbf{A}^\top \mathbf{V}\mathbf{A} \\ \mathbf{V} \\ \log |\mathbf{V}| \end{bmatrix} \cdot \begin{bmatrix} \mathbf{Y}\mathbf{W}\mathbf{X}^\top \\ -\frac{1}{2} \mathbf{X}\mathbf{W}\mathbf{X}^\top \\ -\frac{1}{2} \mathbf{Y}\mathbf{W}\mathbf{Y}^\top \\ \frac{1}{2} \sum_{n=1}^N w_n \end{bmatrix} \right\},$$

where w_n are the weights and $\mathbf{W} = \text{diag}(w_n)$ is the diagonal weight matrix. The data matrices \mathbf{X} and \mathbf{Y} are of size $d \times N$ and $m \times N$ respectively. The conjugate prior $p(\mathbf{A}, \mathbf{V})$ is a matrix-normal-Wishart with zero mean

$$p(\mathbf{A}, \mathbf{V}) = N(\mathbf{A}|\mathbf{0}, \mathbf{V}, \mathbf{K}_0) W(\mathbf{V}|\boldsymbol{\Psi}_0, \nu_0) \\ \propto \exp \left\{ \begin{bmatrix} \mathbf{0} \\ -\frac{1}{2} \mathbf{K}_0 \\ -\frac{1}{2} \boldsymbol{\Psi}_0^{-1} \\ \frac{1}{2}(\nu_0 - m - 1 + d) \end{bmatrix} \cdot \begin{bmatrix} \mathbf{V}\mathbf{A} \\ \mathbf{A}^\top \mathbf{V}\mathbf{A} \\ \mathbf{V} \\ \log |\mathbf{V}| \end{bmatrix} \right\}.$$

The posterior $q(\boldsymbol{\mu}, \boldsymbol{\Lambda})$ is matrix-normal-Wishart

$$q(\mathbf{A}, \mathbf{V}) = N(\mathbf{A}|\mathbf{M}, \mathbf{V}, \mathbf{K}) W(\mathbf{V}|\boldsymbol{\Psi}, \nu) \\ \propto \exp \left\{ \begin{bmatrix} \mathbf{Y}\mathbf{W}\mathbf{X}^\top \\ -\frac{1}{2}(\mathbf{K}_0 + \mathbf{X}\mathbf{W}\mathbf{X}^\top) \\ -\frac{1}{2}(\boldsymbol{\Psi}_0^{-1} + \mathbf{Y}\mathbf{W}\mathbf{Y}^\top) \\ \frac{1}{2}(\nu_0 - m - 1 + d + \sum_{n=1}^N w_n) \end{bmatrix} \cdot \begin{bmatrix} \mathbf{V}\mathbf{A} \\ \mathbf{A}^\top \mathbf{V}\mathbf{A} \\ \mathbf{V} \\ \log |\mathbf{V}| \end{bmatrix} \right\}.$$

The mode mapping and precision of a matrix-normal-Wishart are $\hat{\mathbf{A}} = \mathbf{M}$ and $\hat{\boldsymbol{\Lambda}} = (\nu - m)\boldsymbol{\Psi}$, respectively. The posterior parameters necessary for this computation are

$$\mathbf{K} = \mathbf{K}_0 + \mathbf{X}\mathbf{W}\mathbf{X}^\top, \\ \mathbf{M} = \mathbf{Y}\mathbf{W}\mathbf{X}^\top \mathbf{K}^{-1}, \\ \nu = \nu_0 + \sum_{n=1}^N w_n, \\ \boldsymbol{\Psi} = (\boldsymbol{\Psi}_0^{-1} + \mathbf{Y}\mathbf{W}\mathbf{Y}^\top - \mathbf{M}\mathbf{K}\mathbf{M}^\top)^{-1}.$$

The empirical Bayes gradients of the log-prior are

$$\frac{\partial \log p(\mathbf{A}, \mathbf{V})}{\partial \mathbf{K}_0} = \frac{d}{2} \mathbf{K}^{-\top} - \frac{1}{2} \mathbf{A}\mathbf{V}\mathbf{A}^\top, \\ \frac{\partial \log p(\mathbf{A}, \mathbf{V})}{\partial \boldsymbol{\Psi}_0} = \frac{1}{2} (\boldsymbol{\Psi}_0^{-1} \boldsymbol{\Lambda} \boldsymbol{\Psi}_0^{-1})^\top - \frac{\nu_0}{2} (\boldsymbol{\Psi}_0^{-1})^\top, \\ \frac{\partial \log p(\mathbf{A}, \mathbf{V})}{\partial \nu_0} = \frac{1}{2} (\log |\boldsymbol{\Lambda}| - d \log(2) - \log |\boldsymbol{\Psi}| - \psi(\frac{\nu_0}{2})).$$

APPENDIX III HYBRID CONTROL OPTIMIZATION

The Lagrangian L of the optimization problem described in Equations (1c)-(1d) is formulated as follows

$$\begin{aligned}
 L = & \sum_{\mathbf{z}} \iint r(\mathbf{x}, \mathbf{u}, \mathbf{z}) p(\mathbf{x}, \mathbf{u}, \mathbf{z}) \, d\mathbf{u} \, d\mathbf{x} \\
 & + \sum_{\mathbf{z}'} \int V(\mathbf{x}', \mathbf{z}') \left(- \int p(\mathbf{x}', \mathbf{u}, \mathbf{z}') \, d\mathbf{u} \right. \\
 & + (1 - \vartheta) \sum_{\mathbf{z}} \iint p(\mathbf{x}, \mathbf{u}, \mathbf{z}) \mu_1(\mathbf{x}', \mathbf{z}') \, d\mathbf{u} \, d\mathbf{x} \\
 & \left. + \vartheta \sum_{\mathbf{z}} \iint p(\mathbf{x}, \mathbf{u}, \mathbf{z}) p(\mathbf{x}', \mathbf{z}' | \mathbf{x}, \mathbf{u}, \mathbf{z}) \, d\mathbf{u} \, d\mathbf{x} \right) d\mathbf{x}' \\
 & + \lambda \left(1 - \sum_{\mathbf{z}} \iint p(\mathbf{x}, \mathbf{u}, \mathbf{z}) \, d\mathbf{u} \, d\mathbf{x} \right) \\
 & + \eta \left(\epsilon - \text{KL}(p(\mathbf{x}, \mathbf{u}, \mathbf{z}) \parallel q(\mathbf{x}, \mathbf{u}, \mathbf{z})) \right),
 \end{aligned}$$

where λ is the multiplier associated with Equation (1d).

REFERENCES

- [1] I. Fantoni and R. Lozano, *Nonlinear Control for Underactuated Mechanical Systems*, 2002.
- [2] J. Kober, J. A. Bagnell, and J. Peters, "Reinforcement learning in robotics: A survey," *The International Journal of Robotics Research*, 2013.
- [3] V. Mnih, K. Kavukcuoglu, D. Silver, A. A. Rusu, J. Veness, M. G. Bellemare, A. Graves, M. Riedmiller, A. K. Fidjeland, G. Ostrovski *et al.*, "Human-level control through deep reinforcement learning," *Nature*, 2015.
- [4] M. Deisenroth and C. E. Rasmussen, "PILCO: A model-based and data-efficient approach to policy search," in *International Conference on Machine Learning*, 2011.
- [5] S. Levine, C. Finn, T. Darrell, and P. Abbeel, "End-to-end training of deep visuomotor policies," *The Journal of Machine Learning Research*, 2016.
- [6] D. Hafner, T. Lillicrap, I. Fischer, R. Villegas, D. Ha, H. Lee, and J. Davidson, "Learning latent dynamics for planning from pixels," in *International Conference on Machine Learning*, 2019.
- [7] J. Schulman, S. Levine, P. Abbeel, M. Jordan, and P. Moritz, "Trust region policy optimization," in *International Conference on Machine Learning*, 2015.
- [8] T. P. Lillicrap, J. J. Hunt, A. Pritzel, N. Heess, T. Erez, Y. Tassa, D. Silver, and D. Wierstra, "Continuous control with deep reinforcement learning," *arXiv preprint arXiv:1509.02971*, 2015.
- [9] T. Haarnoja, A. Zhou, P. Abbeel, and S. Levine, "Soft actor-critic: Off-policy maximum entropy deep reinforcement learning with a stochastic actor," in *International Conference on Machine Learning*, 2018.
- [10] D. Liberzon, *Calculus of Variations and Optimal Control Theory: A Concise Introduction*, 2011.
- [11] —, *Switching in Systems and Control*, 2003.
- [12] W. M. Haddad, V. Chellaboina, and S. G. Nersisov, "Impulsive and hybrid dynamical systems," *Princeton Series in Applied Mathematics*, 2006.
- [13] R. Goebel, R. G. Sanfelice, and A. R. Teel, *Hybrid Dynamical Systems: Modeling, Stability, and Robustness*, 2012.
- [14] F. Borrelli, A. Bemporad, and M. Morari, *Predictive Control for Linear and Hybrid Systems*, 2017.
- [15] Z. Ghahramani and G. E. Hinton, "Variational learning for switching state-space models," *Neural Computation*, 2000.
- [16] M. J. Beal, "Variational algorithms for approximate Bayesian inference," Ph.D. dissertation, University College London, 2003.
- [17] E. Fox, "Bayesian nonparametric learning of complex dynamical phenomena," Ph.D. dissertation, Massachusetts Institute of Technology, 2009.
- [18] S. W. Linderman, M. J. Johnson, A. C. Miller, R. P. Adams, D. M. Blei, and L. Paninski, "Bayesian learning and inference in recurrent switching linear dynamical systems," in *International Conference on Artificial Intelligence and Statistics*, 2017.
- [19] G. F. Montufar, R. Pascanu, K. Cho, and Y. Bengio, "On the number of linear regions of deep neural networks," in *Advances in Neural Information Processing Systems*, 2014.
- [20] R. Arora, A. Basu, P. Mianjy, and A. Mukherjee, "Understanding deep neural networks with rectified linear units," *arXiv preprint arXiv:1611.01491*, 2016.
- [21] X. Pan and V. Srikumar, "Expressiveness of rectifier networks," in *International Conference on Machine Learning*, 2016.
- [22] T. Serra, C. Tjandraatmadja, and S. Ramalingam, "Bounding and counting linear regions of deep neural networks," *arXiv preprint arXiv:1711.02114*, 2017.
- [23] P. Petersen and F. Voigtlaender, "Optimal approximation of piecewise smooth functions using deep ReLU neural networks," *Neural Networks*, 2018.
- [24] J.-P. Forestier and P. Varaiya, "Multilayer control of large Markov chains," *IEEE Transactions on Automatic Control*, 1978.
- [25] S.-H. Lin, "Exploiting structure for planning and control," Ph.D. dissertation, Brown University, 1997.
- [26] M. Hauskrecht, N. Meuleau, L. P. Kaelbling, T. L. Dean, and C. Boutilier, "Hierarchical solution of Markov decision processes using macro-actions," in *Conference on Uncertainty in Artificial Intelligence*, 1998.
- [27] T. G. Dietterich, "State abstraction in MAXQ hierarchical reinforcement learning," in *Advances in Neural Information Processing Systems*, 2000.
- [28] H. Abdulsamad and J. Peters, "Hierarchical decomposition of nonlinear dynamics and control for system identification and policy distillation," in *Learning for Dynamics and Control*, 2020.
- [29] F. Borrelli, A. Bemporad, M. Fodor, and D. Hrovat, "An MPC/hybrid system approach to traction control," *IEEE Transactions on Control Systems Technology*, 2006.
- [30] P. Menchinelli and A. Bemporad, "Hybrid model predictive control of a solar air conditioning plant," *European Journal of Control*, 2008.
- [31] A. Bemporad and S. Di Cairano, "Optimal control of discrete hybrid stochastic automata," in *International Workshop on Hybrid Systems: Computation and Control*, 2005.
- [32] C. G. Cassandras and J. Lygeros, *Stochastic Hybrid Systems*, 2006.
- [33] S. Paoletti, A. L. Juloski, G. Ferrari-Trecate, and R. Vidal, "Identification of hybrid systems: A tutorial," *European Journal of Control*, 2007.
- [34] A. Bemporad, J. Roll, and L. Ljung, "Identification of hybrid systems via mixed-integer programming," in *IEEE Conference on Decision and Control*, 2001.
- [35] A. L. Juloski, S. Weiland, and W. Heemels, "A Bayesian approach to identification of hybrid systems," *IEEE Transactions on Automatic Control*, 2005.
- [36] E. Sontag, "Nonlinear regulation: The piecewise linear approach," *IEEE Transactions on Automatic Control*, 1981.
- [37] F. Zhu and P. J. Antsaklis, "Optimal control of hybrid switched systems: A brief survey," *Discrete Event Dynamic Systems*, 2015.
- [38] A. Bemporad and M. Morari, "Control of systems integrating logic, dynamics, and constraints," *Automatica*, 1999.
- [39] A. Bemporad, F. Borrelli, and M. Morari, "Piecewise linear optimal controllers for hybrid systems," in *American Control Conference*, 2000.
- [40] F. Borrelli, M. Baotic, A. Bemporad, and M. Morari, "An efficient algorithm for computing the state feedback optimal control law for discrete time hybrid systems," in *American Control Conference*, 2003.
- [41] T. Marcucci and R. Tedrake, "Mixed-integer formulations for optimal control of piecewise-affine systems," in *ACM International Conference on Hybrid Systems: Computation and Control*, 2019.
- [42] G. Ackerson and K. Fu, "On state estimation in switching environments," *IEEE Transactions on Automatic Control*, 1970.
- [43] J. D. Hamilton, "Analysis of time series subject to changes in regime," *Journal of Econometrics*, 1990.
- [44] V. Pavlovic, J. M. Rehg, and J. MacCormick, "Learning switching linear models of human motion," in *Advances in Neural Information Processing Systems*, 2001.
- [45] S. M. Oh, J. M. Rehg, T. Balch, and F. Dellaert, "Data-driven MCMC for learning and inference in switching linear dynamic systems," in *National Conference on Artificial Intelligence*, 2005.
- [46] B. Mesot and D. Barber, "Switching linear dynamical systems for noise robust speech recognition," *IEEE Transactions on Audio, Speech, and Language Processing*, 2007.

- [47] D. Koller, N. Friedman, and F. Bach, *Probabilistic Graphical Models: Principles and Techniques*, 2009.
- [48] U. N. Lerner, "Hybrid Bayesian networks for reasoning about complex systems," Ph.D. dissertation, Stanford University, 2002.
- [49] M. D. Escobar and M. West, "Bayesian density estimation and inference using mixtures," *Journal of the American Statistical Association*, 1995.
- [50] C. E. Rasmussen, "The infinite Gaussian mixture model," in *Advances in Neural Information Processing Systems*, 1999.
- [51] M. J. Beal, Z. Ghahramani, and C. E. Rasmussen, "The infinite hidden Markov model," in *Advances in Neural Information Processing Systems*, 2002.
- [52] Y. W. Teh, M. I. Jordan, M. J. Beal, and D. M. Blei, "Sharing clusters among related groups: Hierarchical Dirichlet processes," in *Advances in Neural Information Processing Systems*, 2005.
- [53] E. Fox, E. B. Sudderth, M. I. Jordan, and A. S. Willsky, "Nonparametric Bayesian learning of switching linear dynamical systems," in *Advances in Neural Information Processing Systems*, 2009.
- [54] D. P. Kingma and M. Welling, "Auto-encoding variational Bayes," *arXiv preprint arXiv:1312.6114*, 2013.
- [55] P. Becker-Ehmck, J. Peters, and P. Van Der Smagt, "Switching linear dynamics for variational Bayes filtering," in *International Conference on Machine Learning*, 2019.
- [56] A. G. Barto and S. Mahadevan, "Recent advances in hierarchical reinforcement learning," *Discrete Event Dynamic Systems*, 2003.
- [57] R. E. Parr, "Hierarchical control and learning for Markov decision processes," Ph.D. dissertation, University of California Berkeley, 1998.
- [58] D. Precup, "Temporal abstraction in reinforcement learning," Ph.D. dissertation, University of Massachusetts Amherst, 2000.
- [59] D. Andre and S. J. Russell, "State abstraction for programmable reinforcement learning agents," in *National Conference on Artificial Intelligence*, 2002.
- [60] R. S. Sutton, D. Precup, and S. Singh, "Between MDPs and semi-MDPs: A framework for temporal abstraction in reinforcement learning," *Artificial Intelligence*, 1999.
- [61] —, "Intra-option learning about temporally abstract actions," in *International Conference on Machine Learning*, 1998.
- [62] S. J. Bradtke and M. O. Duff, "Reinforcement learning methods for continuous-time Markov decision problems," in *Advances in Neural Information Processing Systems*, 1995.
- [63] M. Huber and R. A. Grupen, "Learning to coordinate controllers-reinforcement learning on a control basis," in *International Joint Conferences on Artificial Intelligence*, 1997.
- [64] M. Huber, "A hybrid architecture for adaptive robot control," Ph.D. dissertation, University of Massachusetts Amherst, 2000.
- [65] G. Konidaris and A. G. Barto, "Skill discovery in continuous reinforcement learning domains using skill chaining," in *Advances in Neural Information Processing Systems*, 2009.
- [66] D. J. Mankowitz, T. A. Mann, and S. Mannor, "Adaptive skills adaptive partitions (ASAP)," in *Advances in Neural Information Processing Systems*, 2016.
- [67] C. Daniel, H. Van Hoof, J. Peters, and G. Neumann, "Probabilistic inference for determining options in reinforcement learning," *Machine Learning*, 2016.
- [68] P.-L. Bacon, J. Harb, and D. Precup, "The option-critic architecture," in *AAAI Conference on Artificial Intelligence*, 2017.
- [69] M. Smith, H. Hoof, and J. Pineau, "An inference-based policy gradient method for learning options," in *International Conference on Machine Learning*, 2018.
- [70] L. Li, T. J. Walsh, and M. L. Littman, "Towards a unified theory of state abstraction for MDPs," in *International Symposium on Artificial Intelligence and Mathematics*, 2006.
- [71] R. Akrouf, F. Veiga, J. Peters, and G. Neumann, "Regularizing reinforcement learning with state abstraction," in *IEEE/RSJ International Conference on Intelligent Robots and Systems*, 2018.
- [72] S. Calinon, F. D'halluin, E. L. Sauser, D. G. Caldwell, and A. G. Billard, "Learning and reproduction of gestures by imitation," *IEEE Robotics & Automation Magazine*, 2010.
- [73] M. Burke, Y. Hristov, and S. Ramamoorthy, "Hybrid system identification using switching density networks," in *Conference on Robot Learning*, 2020.
- [74] A. Sosc, A. M. Zoubir, and H. Koepl, "A Bayesian approach to policy recognition and state representation learning," *IEEE Transactions on Pattern Analysis and Machine Intelligence*, 2017.
- [75] D. Barber, "Expectation correction for smoothed inference in switching linear dynamical systems," *Journal of Machine Learning Research*, 2006.
- [76] M. H. Davis, *Markov Models and Optimization*, 1993.
- [77] Z. Ghahramani and M. I. Jordan, "Factorial hidden Markov models," *Machine Learning*, 1997.
- [78] D. Barber, *Bayesian Reasoning and Machine Learning*, 2012.
- [79] J. Peters, K. Mülling, and Y. Altun, "Relative entropy policy search," in *AAAI Conference on Artificial Intelligence*, 2010.
- [80] H. Van Hoof, J. Peters, and G. Neumann, "Learning of non-parametric control policies with high-dimensional state features," in *International Conference on Artificial Intelligence and Statistics*, 2015.
- [81] B. Belousov and J. Peters, "f-Divergence constrained policy improvement," *arXiv preprint arXiv:1801.00056*, 2017.
- [82] S. Kullback and R. A. Leibler, "On information and sufficiency," *The Annals of Mathematical Statistics*, 1951.
- [83] M. L. Puterman, *Markov Decision Processes: Discrete Stochastic Dynamic Programming*, 2014.
- [84] S. Boyd and L. Vandenberghe, *Convex Optimization*, 2004.
- [85] S. M. Ross, *Introduction to Probability Models*, 2014.
- [86] D. F. Crouse, P. Willett, K. Pattipati, and L. Svensson, "A look at Gaussian mixture reduction algorithms," in *International Conference on Information Fusion*, 2011.
- [87] M. Deisenroth, G. Neumann, and J. Peters, "A survey on policy search for robotics," *Foundations and Trends® in Robotics*, 2013.
- [88] J. Schulman, F. Wolski, P. Dhariwal, A. Radford, and O. Klimov, "Proximal policy optimization algorithms," *arXiv preprint arXiv:1707.06347*, 2017.
- [89] L. E. Baum, T. Petrie, G. Soules, and N. Weiss, "A maximization technique occurring in the statistical analysis of probabilistic functions of Markov chains," *The Annals of Mathematical Statistics*, 1970.
- [90] A. P. Dempster, N. M. Laird, and D. B. Rubin, "Maximum likelihood from incomplete data via the EM algorithm," *Journal of the Royal Statistical Society*, 1977.
- [91] L. R. Rabiner, "A tutorial on hidden Markov models and selected applications in speech recognition," *IEEE*, 1989.
- [92] Y. Bengio and P. Frasconi, "An input-output HMM architecture," in *Advances in Neural Information Processing Systems*, 1995.
- [93] L. Bottou, "Online learning and stochastic approximations," *Online Learning in Neural Networks*, 1998.
- [94] A. Gelman, H. S. Stern, J. B. Carlin, D. B. Dunson, A. Vehtari, and D. B. Rubin, *Bayesian Data Analysis*, 2013.
- [95] J. S. Maritz and T. Lwin, "Empirical Bayes methods," *Monographs on Statistics and Applied Probability*, 1989.
- [96] K. P. Murphy, *Machine Learning: A Probabilistic Perspective*, 2012.
- [97] H. Robbins and S. Monro, "A stochastic approximation method," *The Annals of Mathematical Statistics*, 1951.
- [98] A. Gelman, "Prior distributions for variance parameters in hierarchical models," *Bayesian Analysis*, 2006.
- [99] S. Hochreiter and J. Schmidhuber, "Long short-term memory," *Neural Computation*, 1997.
- [100] A. Rahimi and B. Recht, "Random features for large-scale kernel machines," in *Advances in Neural Information Processing Systems*, 2008.
- [101] M. J. Wainwright and M. I. Jordan, "Graphical models, exponential families, and variational inference," *Foundations and Trends in Machine Learning*, 2008.